69. Broutman, L.J. and Agarwal, B.D. 1974. A theoretical study of the effect of an interfacial layer on the properties of composites. *Polymer Engineering and Science*, 14(8), 581–588.
70. Schwartz, H.S. and Hartness, T. 1987. Effect of fiber coatings on interlaminar fracture toughness of composites, in Johnston, N.J. ed., *Toughened Composites*, ASTM STP 937, pp. 150–178. American Society for Testing and Materials, Philadelphia, PA.
71. Browning, C.E. and Schwartz, H.S. 1986. Delamination resistant composite concepts, in Whitney, J.M. ed., *Composite Materials: Testing and Design (Seventh Conference)*, ASTM STP 893, pp. 256–265. American Society for Testing and Materials, Philadelphia, PA.
72. Mignery, L.A., Tan, T.M., and Sun, C.T. 1985. The use of stitching to suppress delamination in laminated composites, in Johnson, W.S. ed., *Delamination and Debonding of Materials*, ASTM STP 876, pp. 371–385. American Society for Testing and Materials, Philadelphia, PA.
73. Garcia, R., Evans, R.E., and Palmer, R.J. 1987. Structural property improvements through hybridized composites, in Johnston, N.J. ed., *Toughened Composites*, ASTM STP 937, pp. 397–412. American Society for Testing and Materials, Philadelphia PA.
74. Kim, J.K. and Mai, Y.W. 1991. High stretch, high fracture toughness fibre composites with interface control — a review. *Composites Science and Technology*, 41, 333–378.
75. Yan, W., Liu, H.-Y., and Mai, Y.-W. 2003. Numerical study on the Mode I delamination toughness of z-pinned laminates. *Composites Science and Technology*, 63(10), 1481–1493.
76. Byrd, L.W. and Birman, V. 2006. Effectiveness of z-pins in preventing delamination of co-cured composite joints on the example of a double cantilever test. *Composites Part B Engineering*, 37(4–5), 365–378.
77. Cartie, D.D.R., Troulis, M., and Partridge, I.K. 2006. Delamination of z-pinned carbon fibre reinforced laminates. *Composites Science and Technology*, 66(6), 855–861.
78. Mouritz, A.P., Baini, C., and Herszberg, I. 1999. Mode I interlaminar fracture toughness properties of advanced textile fiberglass composites. *Composites Part A Applied Science and Manufacturing*, 30A(7), 859–870.
79. Yau, S.-S., Chou, T.-W., and Ko, F.K. 1986. Flexural and axial compressive failures of three-dimensionally braided composite I-beams. *Composites*, 17(3), 227–232.
80. Allix, O. and Johnson, A. eds. 2006. Advances in statics and dynamics of delamination. *Composites Science and Technology* (special issue), 66(6), 695–862.

10

Mechanical Testing of Composites and Their Constituents

10.1 Introduction

The purpose of this chapter is to review briefly the most widely used methods for mechanical testing of composite materials and their constituents. In previous chapters, the emphasis has been on the development of analytical models for mechanical behavior of composite materials. The usefulness of such models depends heavily on the availability of measured intrinsic mechanical property data to use as input. In addition, some aspects of mechanical behavior of composites are so complex that the feasibility of proper analytical modeling is questionable, and the experimental approach may be the only acceptable solution. Much of our knowledge about the special nature of composite behavior has been derived from experimental observations. The measurement of mechanical properties is also an important element of the quality control and quality assurance processes associated with the manufacture of composite materials and structures.

Due to the special characteristics of composites, such as anisotropy, coupling effects, and the variety of possible failure modes, it has been found that the mechanical test methods that are used for conventional metallic materials are usually not applicable to composites. Thus, the development and evaluation of new test methods for composites have been, and continues to be, a major challenge for the experimental mechanics community. The technology associated with composite test methods and test equipment has become just as sophisticated as that associated with the corresponding analytical methods. Many of these test methods have evolved into standards that have been adopted by ASTM International, formerly the American Society for Testing and Materials. The ASTM standards for testing of polymer matrix and metal matrix composites and their constituents are compiled mainly in ASTM Volume 15.03 [1], while the standards for testing ceramic matrix composites are compiled mainly in ASTM Volume 15.01 [2]. The emphasis in this chapter will

be on mechanical testing of polymer matrix composites. Several useful books that are devoted to experimental characterization of composites have been published [3,4], and all of the ASTM standards for testing polymer matrix composites are conveniently listed in the ASTM D4762-04 Standard Guide for Testing Polymer Matrix Composite Materials [5].

10.2 Measurement of Constituent Material Properties

From the earlier discussion of various micromechanical models, it should be obvious that experimentally determined constituent material properties are required as input to these models. Since the development of new composites depends so heavily on the development of new fiber and matrix materials, constituent material tests are often used for screening new materials before composites are made from them. This section deals with the test methods that are used to measure the mechanical properties of fiber and matrix materials.

10.2.1 Fiber Tests

The tensile strength and Young's modulus of individual reinforcing fibers under static longitudinal loading may be determined by the ASTM D C1557.03$^{\varepsilon 1}$ standard test method [6]. As shown in figure 10.1, the fiber specimen is adhesively bonded to a thin paper, compliant metal, or plastic backing strip that has a central longitudinal slot or hole. Once the specimen is clamped in the grips of the tensile testing machine, the backing

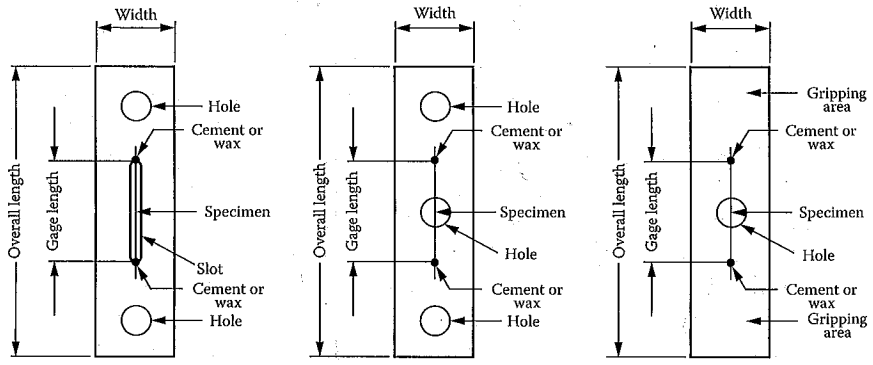

FIGURE 10.1
Different ways of mounting fiber specimens on backing strip. (From ASTM Standard C 1557-03$^{\varepsilon 1}$. Copyright ASTM International. Reprinted with permission.)

strip is burned or cut away, so that the filament transmits all the applied tensile load. The specimen is pulled to failure, the load and elongation are recorded, and the tensile strength and modulus are calculated from the usual formulas. For such small specimens, however, it is important to correct the measured compliance by subtracting out the system compliance. The system compliance can be determined by testing specimens of different gage lengths, plotting the compliance versus gage length, and extrapolating the curves to zero gage length. The compliance corresponding to zero gage length is assumed to be the system compliance [6]. This and other techniques for the measurement of single graphite fiber, longitudinal tensile properties have been evaluated by McMahon [7].

Resin-impregnated and consolidated yarns, strands, rovings, and tows of carbon and graphite fibers may be tested by using ASTM D4018-99 [8]. The impregnating resin is used to produce a rigid specimen that is easier to handle and test than a loose bundle of yarn and that should ensure uniform loading of the fibers in the bundle. The specimen test procedure is similar to that used in C1557.03$^{\varepsilon 1}$, except that the tensile strength and modulus are calculated on the basis of the fiber stress, not the stress in the resin-impregnated strand. It is important to observe and record the failure mode, particularly any atypical failure modes (fig. 10.2).

The longitudinal modulus of single fibers has also been directly measured by Tsai and Daniel [9], who clamped the fiber specimen on each end and optically measured the transverse deflection of the fiber at midspan as small incremental weights were suspended transversely from the fiber at midspan. The same apparatus was used to measure the longitudinal coefficient of thermal expansion of fibers.

Direct measurement of fiber properties under longitudinal compressive loading or longitudinal shear loading is very difficult. Such properties may be inferred from matrix and composite test data, however, and these tests will be discussed later in this chapter. As mentioned in chapter 3, the transverse Young's modulus of fibers may also be inferred from matrix and composite test data, but direct measurement is possible. For example, Kawabata [10] has tested fibers in transverse diametral compression using the apparatus shown in figure 10.3. The resulting load–deflection curve is compared with the corresponding load–deflection curve from a theoretical model of the fiber under transverse compression. One of the inputs to the model is the transverse Young's modulus of the fiber, which is used as a curve-fitting parameter to match the predictions with the measurements. Kawabata's measurements on graphite and aramid fibers showed even greater anisotropy than did the inferred properties. Tsai and Daniel [11] used a torsional pendulum to indirectly measure the longitudinal shear modulus of single fibers. The fiber specimen was clamped and vertically suspended from one end and a weight was attached at the bottom end. The weight was set into oscillation as a torsional pendulum,

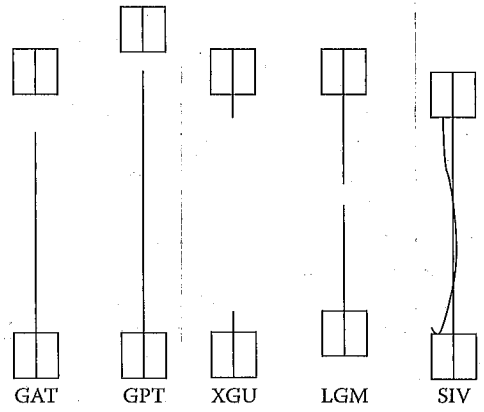

First character		Second character		Third character	
Failure type	Code	Failure area	Code	Failure location	Code
Grip/tab	G	Inside grip/tab	I	Bottom	B
Lateral	L	At grip/tab	A	Top	T
Long splitting (fiber pullout)	S	<1W from grip/tab	W	Middle	M
		Tab pullout	P	Various	V
Explosive	X	Various	V	Unknown	U
Other	O	Unknown	U		

FIGURE 10.2
Different failure modes for resin-impregnated strand test specimens. (From ASTM Standard D4018-99. Copyright ASTM International. Reprinted with permission.)

and the measured frequency of oscillation was used in the frequency equation for the pendulum to solve for the longitudinal shear modulus of the fiber specimen.

Most of the methods described above are used to determine static mechanical properties of fibers. Dynamic test methods involving the use of vibration will be discussed later in this chapter.

10.2.2 Neat Resin Matrix Tests

The tensile yield strength, tensile strength at break, modulus of elasticity, and elongation of neat resin matrix specimens may be determined by using the ASTM D638-03 method for tensile properties of plastics [12]. Several types of "dogbone-shaped" specimens are specified under this standard, depending on the thickness of the available material and whether the material is rigid or nonrigid. Specimens may be fabricated by machining or die cutting from sheets or plates of the material or by molding the resin to the desired shape. For example, the Specimen Types

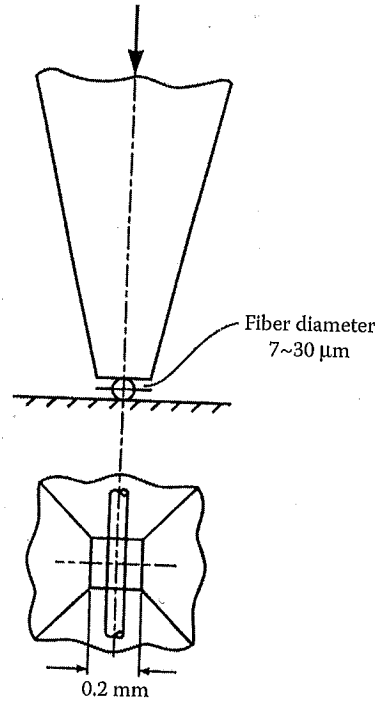

FIGURE 10.3
Diametral compression of fiber for measurement of fiber transverse Young's modulus. (From Kawabata, S. 1989. In Vinson, J.R. ed., *Proceedings of the 4th Japan–U.S. Conference on Composite Materials*, pp. 253–262. CRC Press, Boca Raton, FL. With permission.)

I–V for rigid or semirigid plastics are shown in figure 10.4. Since plastics may be sensitive to temperature and relative humidity, the procedure used to condition specimens should be consistent from one test to another. The so-called "standard laboratory atmosphere" of 23°C (73.4°F) and 50% relative humidity is specified in the ASTM standard D618-05 [13]. Some plastics are also strain-rate sensitive, so the speed of testing should be consistent, as specified in D638-03. The details of the other test conditions and procedures are also given in the standard.

The ASTM D695-02a test method [14] can be used to determine compressive yield strength, compressive strength, and modulus of elasticity of neat resin matrix materials. Out-of-plane buckling failures are avoided by using a very short specimen (fig. 10.5) and a support jig on each side of the specimen (fig. 10.6). In order to generate true axial loading on the specimen without bending, a special compression fixture with a ball-and-socket arrangement is used (fig. 10.7).

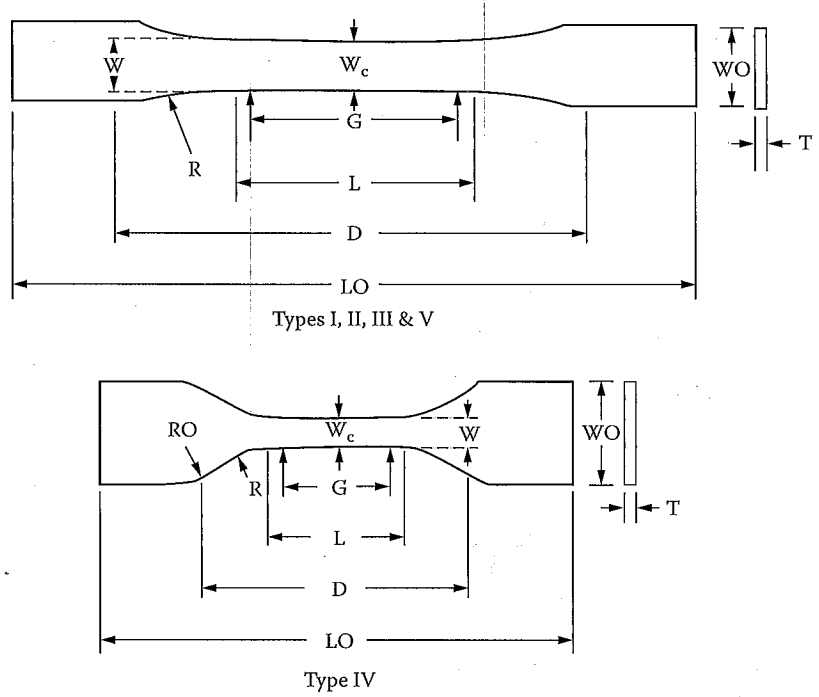

FIGURE 10.4
ASTM D638-03 Type I, II, III, IV and V neat resin tensile specimen geometries. (From ASTM Standard D638-03. Copyright ASTM International. Reprinted with permission).

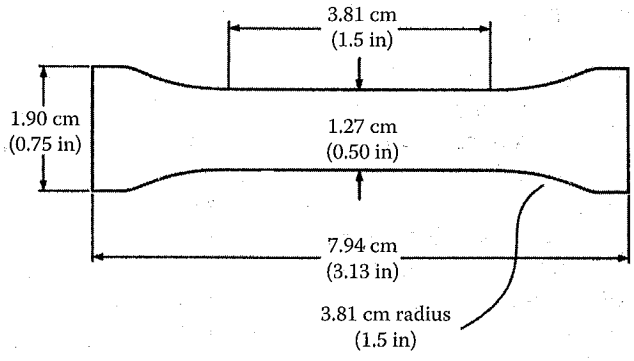

FIGURE 10.5
Neat resin compressive test specimen. (From ASTM Standard D695-02a. Copyright ASTM International. Reprinted with permission.)

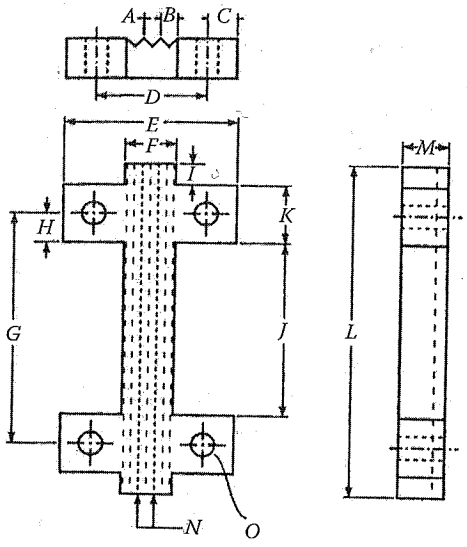

Letter	Metric system	British system
A	0.40 mm	0.0156 in
B	3.18	0.125
C	6.35	0.250
D	23.8	0.9375
E	36.5	1.4375
F	11.1	0.4375
G	50.8	2.00
H	6.35	0.250
I	4.76	0.1875
J	38.1	1.500
K	12.7	0.500
L	73.0	2.875
M	9.53	0.375
N	3.58	0.141
O	4.76 d	0.1875 d

FIGURE 10.6
Support jig for D695-02a compressive test specimen. (From ASTM Standard D695-02a. Copyright ASTM International. Reprinted with permission.)

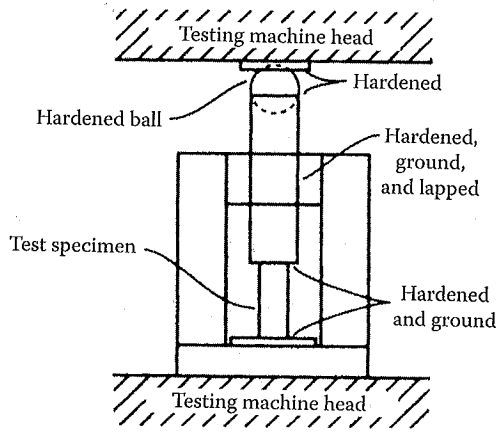

FIGURE 10.7
Compression fixture with ball-and-socket joint to minimize bending. (From ASTM Standard D695-02a. Copyright ASTM International. Reprinted with permission.)

In either the tensile test or the compressive test of the neat resin matrix material, biaxial strain gages can be attached to the specimen so as to measure the longitudinal and transverse strains. The Young's modulus, E, and the Poisson's ratio, ν, can then be determined from the standard definitions of those parameters. If desired, the shear modulus, G, can also be found from the isotropic relationship

$$G = \frac{E}{2(1+\nu)} \tag{10.1}$$

However, Novak and Bert [15] have reported that for some epoxies the values of G found from applying equation (10.1) to either tensile or compressive tests differ substantially from directly measured values of G. Directly measured values of G were determined from a plot of angle of twist versus torque for solid rod torsion tests. It was found that a more accurate calculation of G could be obtained by taking into account differences between tensile and compressive values of E and ν. Their approach was based on the premise that since the elastic strain energy is invariant to a rotation of coordinates, the strain energy for an isotropic material in pure shear along the x, y axes is equal to the strain energy associated with the corresponding biaxial tensile and compressive principal stresses oriented at 45° to the x, y axes. By equating these strain energy terms and using the Hooke's law for an isotropic material with different properties in tension and compression, Novak and Bert showed that the shear modulus, G, can be expressed as

$$\frac{1}{G} = \frac{(1+\nu_t)}{E_t} + \frac{(1+\nu_c)}{E_c} \tag{10.2}$$

where E_t is the Young's modulus from tensile test, E_c the Young's modulus from compressive test, ν_t the Poisson's ratio from tensile test, and, ν_c the Poisson's ratio from compressive test.

This equation, which involves both tensile and compressive properties, was found to give much better agreement with directly measured values of G than did equation (10.1) when equation (10.1) was used with either tensile compressive values of E and ν. It is easily shown that when $E_t = E_c = E$ and $\nu_t = \nu_c = \nu$, equation (10.2) reduces to equation (10.1).

The flexural yield strength, flexural strength, and modulus of elasticity of plastics may be determined by the ASTM D790-03 test method [16]. This test method involves three-point bending (fig. 10.8), and a separate standard D6272-02 describes a four-point bending test. Allowable ranges of radii for the loading noses and recommended specimen dimensions

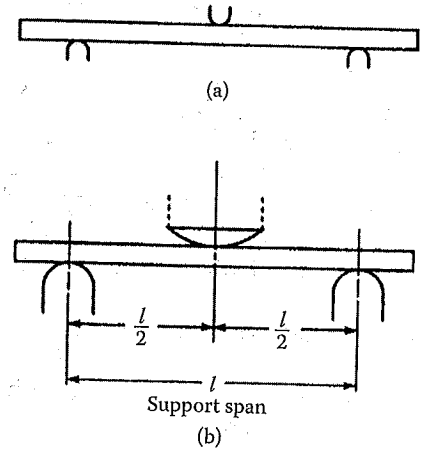

FIGURE 10.8
Three-point bending specimen for flexural properties of neat resin or composite. (From ASTM Standard D790-03. Copyright ASTM International. Reprinted with permission.)

are provided in tables in D790-03 [16]. Test methods for measurement of mechanical properties of other constituents such as sandwich core materials and other constituent properties such as coefficient of thermal expansion, impact, creep, and fatigue response are also given in ref. [1].

10.2.3 Constituent Volume Fraction Measurement

Knowledge of the volume fractions of fiber and matrix materials (and also void fractions, if possible) is essential for use in micromechanical analysis and for quality control during manufacturing of composites. For polymer matrix composites, ASTM standard D3171-99 [17] covers two basic approaches to the measurement of constituent volume fractions. Method I involves removal of the matrix resin from the composite sample using either chemical digestion (with acids or other chemicals) or ignition and burn-off in a furnace, in cases where it is safe to assume that the fibers are unaffected by the resin removal process. For example, by measuring the weight, W_c, and volume, V_c, of a composite sample before resin removal, then measuring the weight, W_f, and volume, V_f, of fibers remaining after resin removal, the fiber weight fraction can be calculated from $w_f = W_f/W_c$, and the fiber volume fraction can be calculated from $v_f = V_f/V_c$. From weight and volume measurements on a separate neat resin matrix sample, the matrix density ρ_m can be determined, then equation (3.6) can be used to determine the matrix volume fraction, v_m. If the void fraction is desired,

involve the use of different chemical mixtures to digest the resin matrix material, depending on the type of polymer matrix resin used in the composite. Procedure G within Method I involves ignition and burn-off of the matrix resin in a furnace if chemical digestion is not feasible. For example, the resin burn-off approach is typically used with glass fibers, but chemical digestion is the preferred approach for carbon fibers, which may suffer mass loss due to oxidation if the resin burn-off approach is used. Method II is based on the assumption that the fiber weight per unit area is known or controlled to within an acceptable degree, and involves measurement of laminate thickness.

A completely different and nondestructive approach to determining constituent volume fractions involves the use of computer-aided image analysis to determine the fiber area fraction in a photomicrograph of a polished composite specimen. A more detailed description of the procedure and equipment used in this approach is described by Adams et al. [3].

10.3 Measurement of Basic Composite Properties

This section is concerned with test methods for measurement of the basic composite mechanical properties that are needed in analysis and design. Methods for measurement of lamina properties such as tensile and compressive strength and stiffness, shear strength and stiffness, flexural strength and stiffness, fiber/matrix interfacial strength, and laminate properties such as interlaminar strength and fracture toughness are discussed. Both direct and indirect methods are reviewed. Direct methods involve the application of uniaxial, shear, or flexural loading to a lamina or laminate specimen so as to determine the basic property that governs the response to such loading. Indirect methods may involve such techniques as "backing out" of lamina properties from tests of laminates. Difficulties encountered in some of these tests are discussed, along with limitations and possible sources of error.

10.3.1 Tensile Tests

Lamina tensile strengths $s_L^{(+)}$ and $s_T^{(+)}$, Young's moduli, E_1 and E_2, and Poisson's ratios, v_{12} and v_{21}, may be measured by testing longitudinal (0°) and transverse (90°) unidirectional specimens according to the ASTM D3039/D3039M-00$^{\varepsilon 2}$ standard test method [18]. The specimen geometry is shown in figure 10.9. Laminated load transfer tabs are adhesively bonded to the ends of the specimen in order that the load may be transferred from the grips of the tensile testing machine to the specimen without

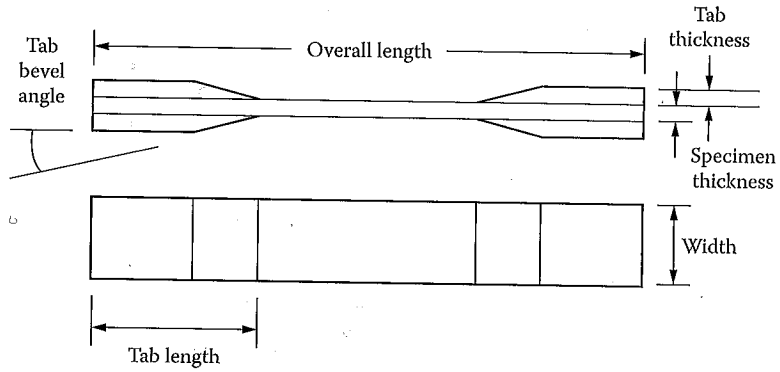

Fiber orientation	Width, mm (in.)	Overall length mm (in.)	Thickness, mm (in.)	Tab length mm (in.)	Tab thickness, mm (in.)	Tab bevel angle (°)
0° unidirectional	15 (0.5)	250 (10.0)	1.0 (0.040)	56 (2.25)	1.5 (0.062)	7 or 90
90° unidirectional	25 (1.0)	175 (7.0)	2.0 (0.080)	25 (1.0)	1.5 (0.062)	90
Balanced and symmetric	25 (1.0)	250 (10.0)	2.5 (0.100)	emery cloth	–	–
Random-discontinuous	25 (1.0)	250 (10.0)	2.5 (0.100)	emery cloth	–	–

FIGURE 10.9
Specimen geometry for ASTM D3030/D3030M-00$^{\varepsilon 2}$ standard tensile test. (Dimensions from ASTM D3030/D3030M-00$^{\varepsilon 2}$. Copyright ASTM International. Reprinted with permission.)

damaging the specimen. Recommended dimensions for 0° and 90° specimens and several types of other laminates are provided in the standard, along with recommended test procedures and calculations. Typical longitudinal and transverse strain data from such a test on a $[0]_8$ graphite/epoxy composite are given in figure 10.10 from [19] for various stresses along with the resulting values of E_1, v_{12}, $s_L^{(+)}$, and $e_L^{(+)}$. These results show the typical fiber-dominated linearity for the longitudinal strain response and a slight nonlinearity in the transverse strain response due to the influence of the matrix.

The D3039/D3039M-00 E2 test method works well for orthotropic specimens because a uniform state of stress is produced across the specimen as it is loaded in tension. However, nonuniformities in the stress distribution may arise when the method is used for off-axis specimens that exhibit shear coupling. Such off-axis tests would typically be used to measure such properties as the off-axis Young's modulus, E_x, and the off-axis tensile strength, $s_x^{(+)}$. Pagano and Halpin [20] showed that a specimen that exhibits shear coupling will deform as shown in figure 10.11(a) if the ends are unconstrained. But if the ends are constrained by clamping fixtures, the shear–coupling effects will produce shear forces and bending

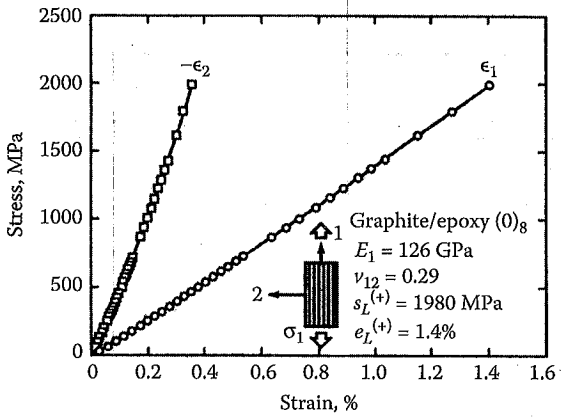

FIGURE 10.10
Longitudinal and transverse strain data at different stresses for $[0]_8$ graphite/epoxy tensile specimen. (From Carlsson, L.A. and Pipes, R.B. 1989. *Experimental Characterization of Advanced Composite Materials*. Prentice-Hall, Inc., Englewood Cliffs, NJ. Reprinted by permission of Prentice-Hall, Englewood Cliffs, NJ.)

moments that distort the specimen, as shown in figure 10.11(b). Thus, in the latter case, the specimen is no longer under a uniform state of stress, and the usual definitions of the engineering constants are not valid. Pagano and Halpin found that the distortion shown in figure 10.11(b)

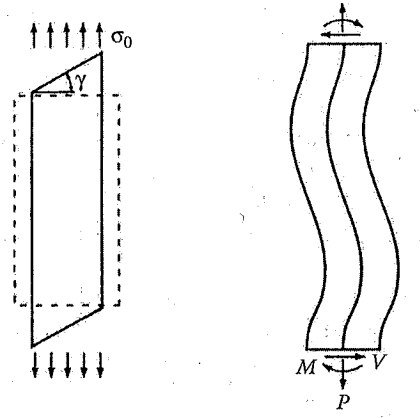

(a) Ends unconstrained (b) Ends clamped

FIGURE 10.11
Effect of end conditions on deformation of an off-axis tensile specimen exhibiting shear coupling. (From Pagano, N.J. and Halpin, J.C 1968. *Journal of Composite Materials*, 2, 18–31. With permission.)

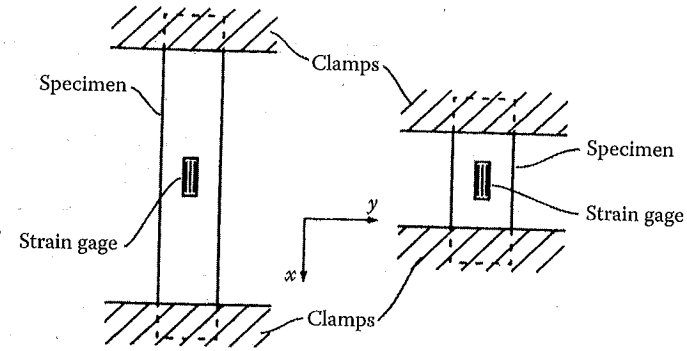

(a) Long, slender specimen (b) Short, wide specimen

FIGURE 10.12
Tensile specimens of different length showing relationship of gage length to specimen length.

decreases with decreasing shear–coupling ratio, $\eta_{x,xy}$ (recall eq. [2.40]) and increasing length-to-width ratio of the specimen. They also suggested that in order to minimize such effects, angle-ply laminates could be used instead of off-axis specimens, or that a test fixture that allowed free rotation of the ends of the specimen could be used with off-axis specimens.

A similar conclusion regarding end constraint effects in off-axis specimens was proposed by Jones [21]. Jones suggested that for long, slender off-axis specimens under a uniaxial stress, as shown in figure 10.12(a), the state of stress in the gage section of the specimen would be approximately

$$\sigma_y = \tau_{xy} = 0 \quad \text{and} \quad \sigma_x = E_x \varepsilon_x \tag{10.3}$$

because the gage length is sufficiently far removed from the effects of the clamped ends. However, in a short, wide specimen (fig. 10.12[b]), the proximity of the clamped ends to the gage length will cause the strains in the gage length to be approximately

$$\varepsilon_y = \gamma_{xy} = 0 \tag{10.4}$$

When these strain conditions are substituted in equation (2.35), the resulting stress condition in the gage length of the short, wide specimen is found to be

$$\sigma_x = \bar{Q}_{11} \varepsilon_x \tag{10.5}$$

The conclusion here is that in the case of a long, slender specimen the off-axis Young's modulus, E_x, is measured. However, in the case of the short, wide specimen the transformed lamina stiffness, $\bar{Q}_{11}$, is measured instead of E_x. For example, Jones [21] points out that for a 30° off-axis test of graphite/epoxy the value of $\bar{Q}_{11}$ is more than 10 times as great as E_x. Thus, the analyses of Pagano and Halpin [20] and Jones [21] lead to the same conclusion regarding the effect of specimen length in off-axis tensile tests.

In the analysis of Jones [21], it is assumed that equation (10.3) is valid when the specimen is "long enough," so that the end effects are not significant in the gage length. The decay of such localized effects with distance away from the source is justified by the use of Saint-Venant's principle. However, Horgan et al. [22–24] have shown that the characteristic decay length over which end effects are significant in orthotropic composites is generally several times greater than the corresponding decay length for isotropic materials. The decay length, λ, which is the distance from the end of the specimen over which the stress decays to $1/e$ of the value of the stress at the end, was found to be

$$\lambda \simeq \frac{b}{2\pi}\sqrt{\frac{E_1}{G_{12}}} \quad \text{as} \quad \frac{G_{12}}{E_1} \to 0 \tag{10.6}$$

for an anisotropic, transversely isotropic, rectangular strip [24], where b is the width of the strip.

In the tests described above, lamina properties are measured directly by testing unidirectional specimens. A different approach involves the use of the classical lamination theory (CLT) to "back out" lamina properties from laminate test data [25,26]. For example, Rawlinson [25] has shown that CLT "back-out" factors for obtaining equivalent 0° tensile strengths from both angle-ply and cross-ply laminates showed good agreement with the corresponding experimentally determined factors for several graphite/epoxy composites. As shown in figure 10.13, Rawlinson's data for the equivalent 0° tensile strength of IM7G/8551-7 graphite/epoxy appear to be nearly the same regardless of whether unidirectional 0° specimens or various cross-ply laminate configurations are used. The one notable exception is the particular case of $[0/90]_{2s}$ cross-ply specimens without load transfer tabs. It is seen in figure 10.13 that the scatter in the data is generally less for the cross-ply specimens and that the data for the cross-ply specimens without load transfer tabs are generally just as good as the data for the corresponding specimens with tabs. Thus, there appears to be considerable potential for cost savings with the tests of untabbed cross-ply specimens.

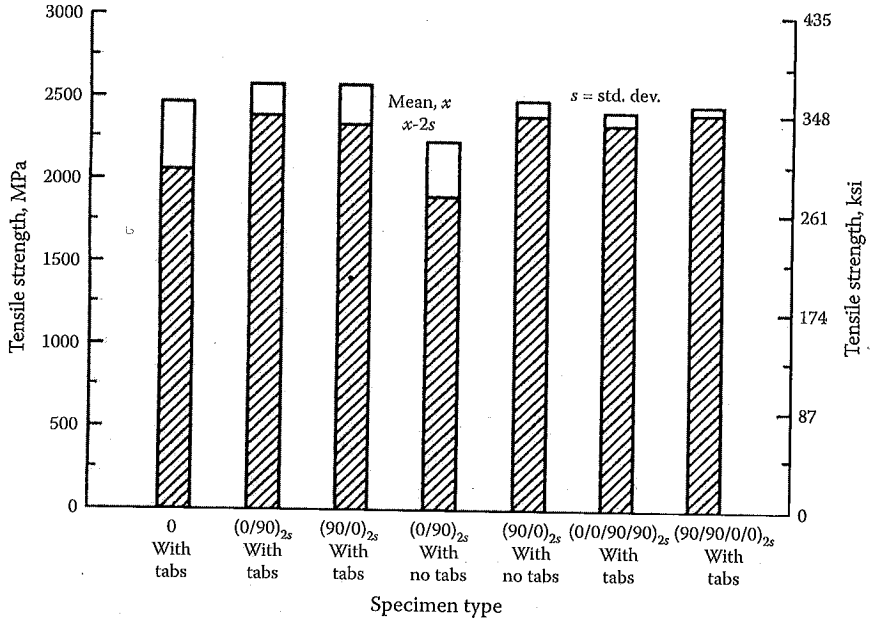

FIGURE 10.13
"Backed out" tensile strength data from seven different laminates of IM7G/8551-7 graphite/epoxy. (From Rawlinson, R.A. 1991. Proceedings of the 36th International SAMPE Symposium and Exhibition, Book 1, pp. 1058–1068. Reprinted by permission of the Society for the Advancement of Material and Process Engineering.)

10.3.2 Compressive Tests

Compression testing has proved to be one of the most interesting and difficult challenges to those concerned with the testing of composites.

There has been considerable discussion in the literature over the years about compression testing of composites, and numerous experimental approaches have been explored [3,27–31]. In general, test methods have been sought, which yield the greatest possible compressive strength, assuming that the greatest values must be closest to the true compressive strength. A great amount of effort has been expended in the design of test fixtures that load the specimen in pure compression and eliminate extraneous failure modes (e.g., global buckling of the specimen and local damage due to load introduction in the grips), which lead to lower apparent compressive strengths. It is ironic that with all the effort that has been devoted to eliminating these other failure modes and achieving true compressive failure, the actual mode of failure of a compressively loaded composite structure in the field is more likely to be something other than

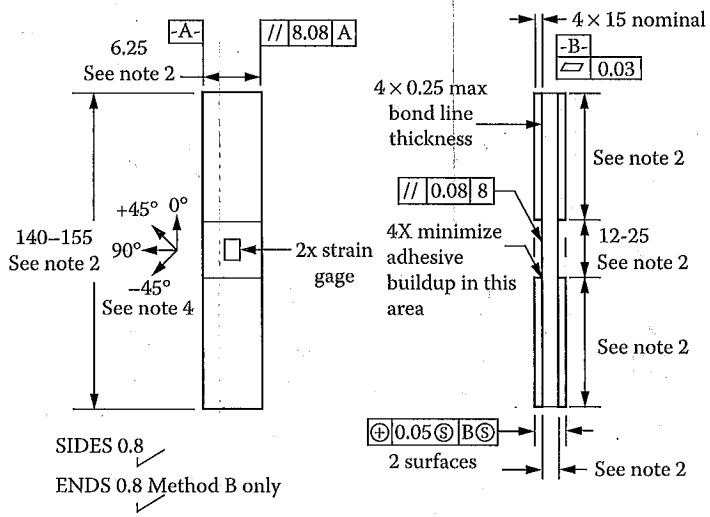

Notes:
1. Drawing interpretation per ANSI Y14.5M-1982 and ANSI/ASME 846.1-1985.
2. See section 8 and table 2 and table 3 of the test standard for values of required or recommended width, thickness, gage length, tab length and overall length.
3. See test standard for values of material, ply orientation, use of tabs, tab material, tab angle, and tab adhesive.
4. Ply orientation tolerance relative to -A- = 0.5°

FIGURE 10.14
Geometry for tabbed compression test specimen. (From ASTM Standard D3410/D3410M-03. Copyright ASTM International. Reprinted with permission.)

pure compressive failure (i.e., it is just as difficult to achieve pure compressive failure in composite structures under service conditions as it is in laboratory test specimens). Three different ASTM standard test methods for compression testing of composites have been published [32–34], and each method will be briefly described in the following.

The ASTM D3410/D3410M-03 test method [32] involves the use of either a tabbed specimen (fig. 10.14) or an untabbed specimen in a special test fixture (fig. 10.15) that has been designed to introduce the compressive load in the specimen by virtue of side loading (i.e., shear transfer to the sides of the specimen from the grips of the test fixture), and to eliminate global buckling of the specimen. The wedge-shaped grips clamp the specimen ever tighter as the compressive load from the testing machine on the test fixture is increased, and all of the compressive load on the specimen comes from this shear transfer. With this fixture, there is no direct compression on the ends of the specimen as with the previously discussed neat resin compression test fixture of ASTM D695-02a.

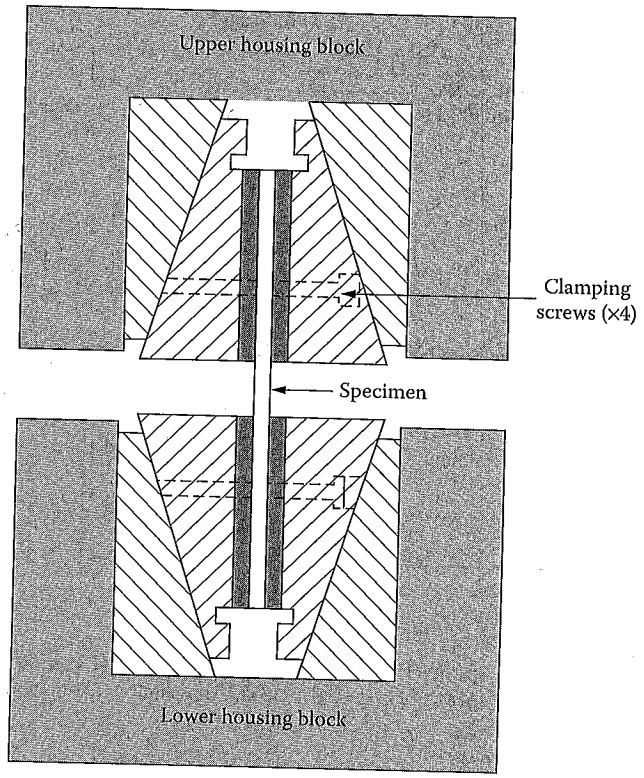

FIGURE 10.15
Cross-section view of ASTM D3410/D3410M-03 compression test fixture. (From ASTM Standard D3410/D3410M-03. Copyright ASTM International. Reprinted with permission.)

The sandwich beam specimen for ASTM D5467-97 [33] shown in figure 10.16 is constructed so that the upper skin consists of the [0] unidirectional composite material of interest. The sandwich beam is bonded together with a structural adhesive, and the specimen is loaded in four-point bending, so that the upper skin is subjected to compressive stress. A honeycomb core material in the sandwich beam provides lateral support for the skin in order to avoid premature buckling of the skin, and thus the failure is due to compressive failure of the skin material.

In a comparison of several test methods that eventually led to the adoption of the current D3410 and D5467 standards, Adsit [35] showed that the methods gave equivalent results for compressive strength and modulus of graphite/epoxy, but that the D695 method for plastics (Figures 10.5–10.7) was inadequate for high-modulus composites. Although all methods gave acceptable results for compression modulus, the D695 method produced premature

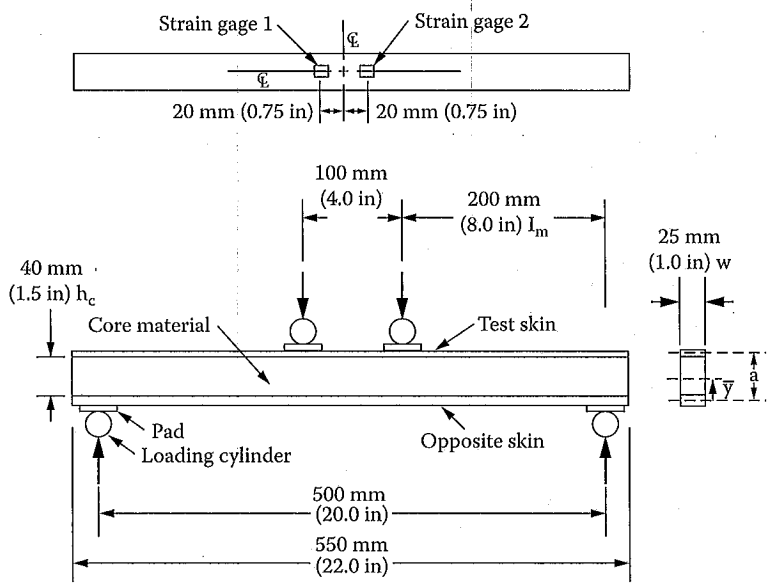

FIGURE 10.16
ASTM D5467/D5467M-97 sandwich beam specimen for face sheet compression. (From ASTM Standard D5467/D5467M-97. Copyright ASTM International. Reprinted with permission.)

The third version of the ASTM standard test methods for compression testing of composites is D6641/D6641M – 01$^{\varepsilon 1}$ [34], the combined loading compression (CLC) test. The CLC fixture (fig. 10.17) involves a combination of direct compression on the ends of an untabbed specimen and shear transfer through side loading to produce pure compression within the gage length of the specimen. Adams et al. [3] have suggested that the CLC method has several advantages over the other two methods. The CLC fixture is relatively simple and compact, no end tabs are required on the specimens, and the ratio of direct compressive load on the ends of the specimen to the shear load on the sides of the specimen can be adjusted for best results.

A number of alternative methods for measurement of compressive modulus and strength have been reported in the literature. The minisandwich specimen [36] is smaller than that used in ASTM D5467 and has a core consisting of the neat resin matrix material instead of a honeycomb material. Compressive properties of the [0] unidirectional lamina can also be "backed out" of [0/90] cross-ply laminate compression test data [37].

The problem of local buckling and the corresponding reduction of in-plane compressive strength after delamination due to transverse impact

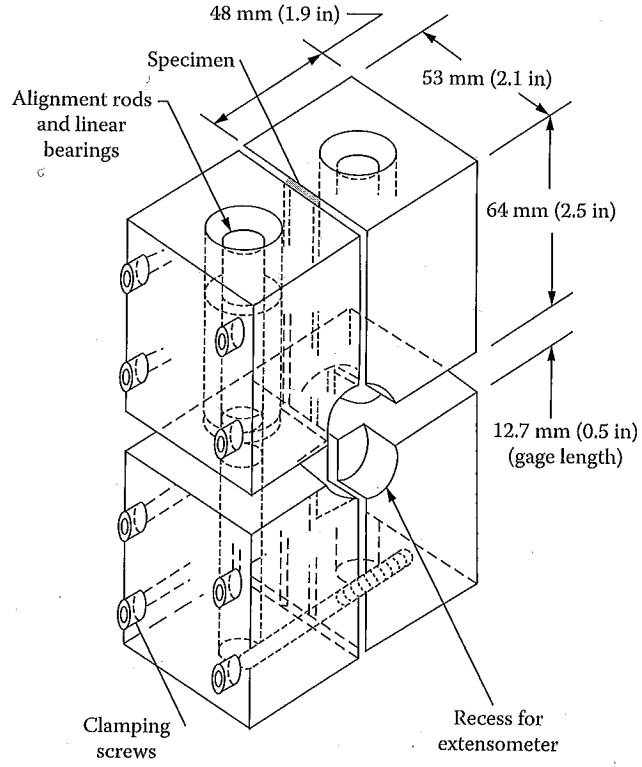

FIGURE 10.17
Test fixture for ASTM D6641/D6641M-01$^{\varepsilon 1}$ CLC test method. (From ASTM Standard D6641/D6641M-01$^{\varepsilon 1}$. Copyright ASTM International. Reprinted with permission.)

have been discussed in chapter 7 (fig. 7.39) and in chapter 9. Concern about this failure mode has led to the development of the compression after impact (CAI) test.

Still more recent work on CAI has led to the development of ASTM Standard D7137/D7137M-05$^{\varepsilon 1}$ on measurement of compressive residual strength properties of damaged polymer matrix composite plates [40], and the test fixture is shown in figure 10.18. First, the test specimens are subjected to either quasistatic indentation damage according to ASTM D6264 or drop-weight impact damage according to ASTM D7136 and then the specimens are subjected to in-plane compression according to ASTM 7137/D7137M-05$^{\varepsilon 1}$. The result of this sequence of tests is data on the compressive residual strength of composite plates with various amounts of statically induced or impact-induced damage.

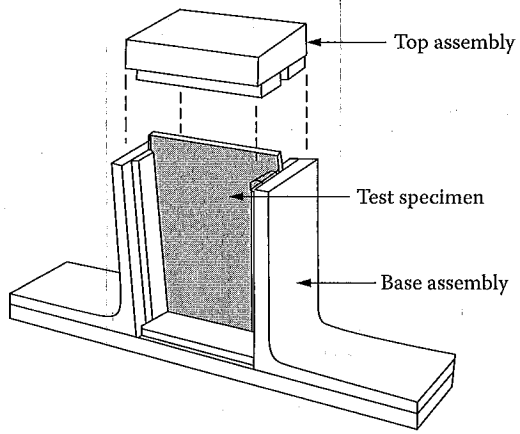

FIGURE 10.18
Test fixture for compressive residual strength of polymer composite plates. (From ASTM D7137/D7137M-05^{e1}. Copyright ASTM International. Reprinted with permission.)

10.3.3 Shear Tests

Shear testing of composites is complicated by the fact that, for an orthotropic material, there are three possible sets of shear properties associated with the three principal material axes (i.e., the in-plane shear modulus G_{12}, the out-of-plane shear moduli G_{13}, and G_{23} and the corresponding shear strengths associated with the 12, 13, and 23 axes). So it should be no surprise that numerous shear test methods have been proposed, that many of them are limited to only one or two of the three possible planes, and that some tests yield only shear modulus or shear strength, but not both. In a very practical, yet quantitative comparison of shear test methods, Adams [41] has reported that at least 14 shear test methods have been developed, 8 of which have been adopted as ASTM standards. Table 10.1 from Adams [41] provides a concise summary of these test methods and their capabilities, listed in decreasing order of frequency of use.

Of the available shear test methods, Adams concludes that only the Iosipescu shear test or V-notched beam test (ASTM D5379/ D5379-05 [42]) and the V-notched rail shear test (ASTM D7078/D7078M-05 [43]) meet all four of the requirements listed in table 10.1. That is, these two methods are the only ones that can presently produce a uniform shear stress state in any of the three possible planes and can be used to determine both the shear strengths and the shear moduli associated with each of the three possible planes. Accordingly, the focus of the present coverage will be on these two methods.

The so-called Iosipescu shear test was first proposed for use with metals in 1967 [44] and was later adapted for use with composites by Adams et al.

TABLE 10.1

Comparison of Shear Test Methods for Composites

Test Method (with ASTM Std. No., if Applicable)	Uniform Shear Stress State	All Three Stress States Practical	Shear Strength Obtained	Shear Stiffness Obtained
Short Beam Shear (D 2344)			■	
Iosipescu Shear (D 5379)	■	■	■	■
±45° Tensile Shear (D 3518)			■	■
Two-Rail Shear (D 4255)			■	■
Three-Rail Shear (D 4255)			■	■
Double-Notched Shear (D 3846)			■	■
Torsion of a Thin Tube (D 5448)	■		■	■
Cross-Beam Sandwich			■	■
Torsion of a Solid Rod			■	■
Four-Point Shear			■	
Picture Frame Shear			■	■
Plate Twist				■
10° Off-Axis (Tensile)			■	■
V-Notched Rail Shear (D 7078)	■	■	■	■

Source: From Adams, D.F., 2005 *High Performance Composites*, 13(5), pp. 9–10.

[45–48]. The Iosipescu test fixture and the corresponding shear and moment diagrams for the specimen are illustrated schematically in figure 10.19, and more details regarding the fixture, specimen dimensions, and test procedures are given in ASTM D5379/ D5379-05 [42]. The action of the test fixture is to produce pure shear loading with no bending at the midspan section of the specimen between the two notches. The average shear stress in that section is simply

$$\tau = \frac{P}{ct} \tag{10.7}$$

where P is the applied load, c is the distance between the roots of the notches, and t is the specimen thickness. No subscripts were used in equation (10.7), because the test method can be used for either in-plane or out-of-plane shear testing, depending on the specimen configuration. Shear strains can be measured using strain gages to measure the normal strains at 45° to the specimen axis, then using the strain transformation equations to find the shear strain (e.g., see Example 2.2). The shear modulus is then the slope of the shear stress–shear strain curve in the elastic region, and the shear strength is the shear stress at failure. In addition to the advantages listed by Adams, the Iosipescu test specimens are small and easily fabricated. This method

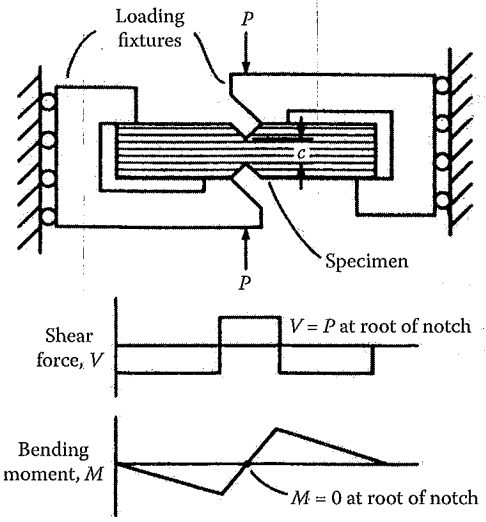

FIGURE 10.19
Iosipescu test fixture with shear and moment diagrams.

Munro [49], who ranked available in-plane shear test methods before the ASTM standard was adopted.

The test fixture for the V-notched rail shear test (ASTM D7078/D7078M-05 [43]) is shown in figure 10.20, and the different possible arrangements for V-notched plate specimens are shown in figure 10.21. Shear stress, shear strain, shear modulus, and shear strength calculations are similar

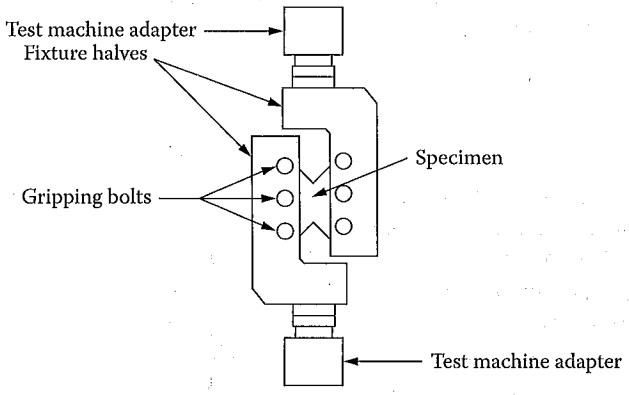

FIGURE 10.20
Test fixture for V-notched rail shear test. (From ASTM Standard D7078/D7078M-05. Copyright ASTM International. Reprinted with permission.)

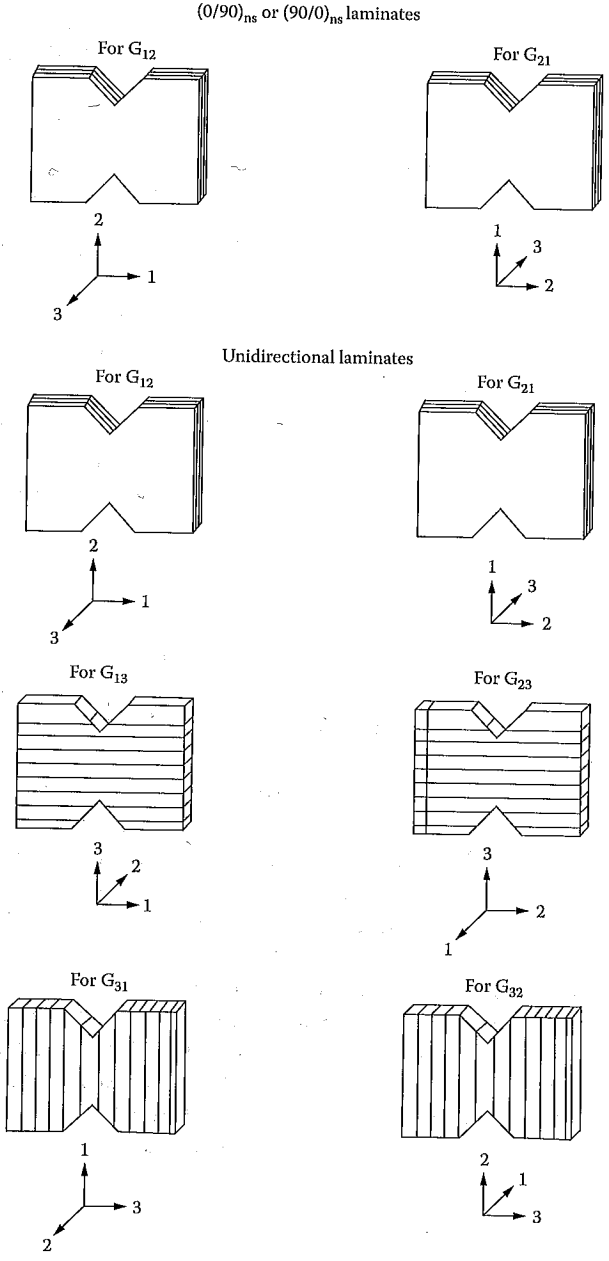

FIGURE 10.21
Different test specimen arrangements for V-notched rail shear test. (From ASTM Standard D7078/D7078M-05. Copyright ASTM International. Reprinted with permission.)

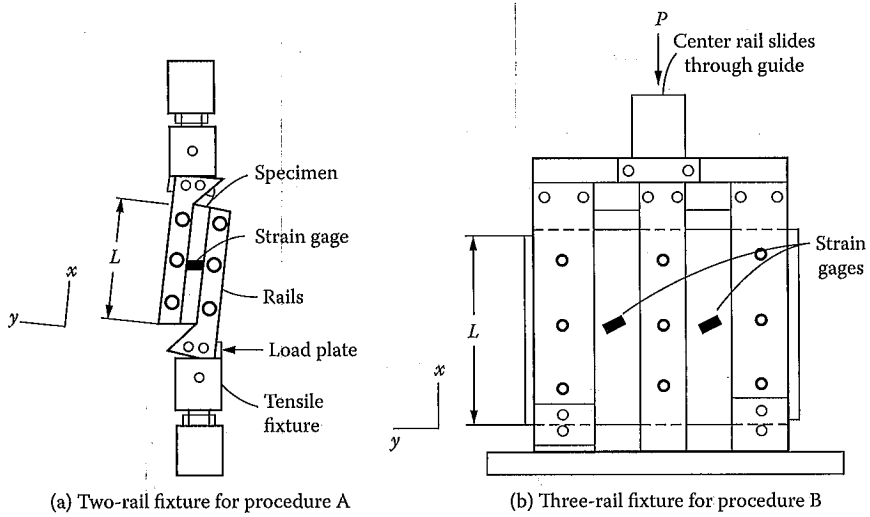

(a) Two-rail fixture for procedure A (b) Three-rail fixture for procedure B

FIGURE 10.22
Rail shear test fixtures. (From ASTM Standard D4255/D4255M-01. Copyright ASTM. Reprinted with permission.)

to those used in the Iosipescu test method. As suggested by Adams [41], this method is the newest of the shear test methods, and, as such, it has not been used extensively yet.

Figure 10.22 shows the original rail shear test method, which can only be used to measure in-plane shear properties. The rail shear test standard, as described in ASTM D4255/D4255M–01 [50], covers two separate procedures. Procedure *A* involves the use of the two-rail fixture shown in figure 10.22(a), whereas procedure *B* requires the use of the three-rail fixture shown in figure 10.22(b). In both procedures, a flat rectangular plate specimen is clamped in between the rail fixtures, and the fixture is subjected to uniaxial loading by a testing machine. The uniaxial loading on the fixture generates in-plane shear loading of the specimen and the resulting strains are monitored by the strain gages shown in figure 10.22(a) and (b). Simple equilibrium requires that the average shear stress along the specimen loading axes (x, y) for procedure A is

$$\tau_{xy} = \frac{P}{Lt} \tag{10.8}$$

where L = specimen length along the x direction, P = applied load along the x direction, and t = specimen thickness, whereas the corresponding

shear stress for procedure B is

$$\tau_{xy} = \frac{P}{2Lt} \tag{10.9}$$

The shear strain along the x,y directions can be determined from the measured normal strain, $\varepsilon_{x'}$, along the x' axis, which is oriented at 45° from the x axis. From the strain transformation relationship for a state of pure shear along the x, y axes, we have

$$\gamma_{xy} = 2\varepsilon_{x'} \tag{10.10}$$

Thus, the shear stress–shear strain data can be generated from equation (10.8) to equation (10.10), and the corresponding modulus and strength can be found from the resulting stress-strain curve.

In-plane shear response can also be determined by testing a thin-walled composite tube in torsion and by measuring the resulting shear strain with a strain gage. If the strain gage is oriented at 45° to the tube axis, and if the applied torque creates a state of pure shear along the x, y axes, equation (10.10) can again be used to determine the shear strain. The shear stress can be estimated from the well-known mechanics of materials formula for a thin-walled tube:

$$\tau_{xy} = \frac{T}{2At} \tag{10.11}$$

where T is the applied torque, t the wall thickness, A the area enclosed by median line, which is equal to πR^2 for cylindrical tube, and R the mean radius of tube.

For the [±45], laminate tensile specimen ASTM D3518/D3518M-94 Reapproved 2001 [51] (fig. 10.23), it can be shown from laminate analysis and a transformation of stresses that the lamina shear stress, τ_{12}, along the

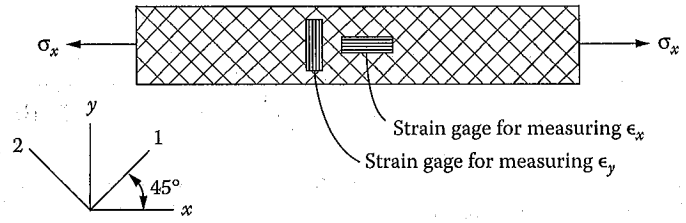

FIGURE 10.23
A $[\pm 45]_s$ laminate tensile specimen for determination of in-plane shear properties.

principal material axes is related to the uniaxial tensile stress, σ_x, acting on the laminate by

$$|\tau_{12}| = \left|\frac{\sigma_x}{2}\right| \tag{10.12}$$

The laminate strains, ε_x^o and ε_y^o, can be transformed to the lamina principal axes at ±45°, so that the magnitude of the lamina shear strain is

$$|\gamma_{12}| = \left|\varepsilon_x^o - \varepsilon_y^o\right| \tag{10.13}$$

where ε_x^o is assumed to be a positive tensile strain and ε_y^o is assumed to be a negative Poisson strain. Thus, measurement of the applied stress, σ_x, and the laminate strains, ε_x^o and ε_y^o, during a tensile test of the $[\pm 45]_s$ laminate enables one to generate the shear stress–shear strain curve for the lamina material. The shear strength and the shear modulus can then be evaluated from this stress–strain curve.

Although the off-axis tensile test is not yet a standard, it is a useful method. For example, a tensile test of an off-axis specimen can be used to determine the off-axis Young's modulus, E_x, as defined by equation (2.38). If the values E_1, E_2, and ν_{12} are known from separate tests of longitudinal and transverse specimens, then the first of equations (2.39) can be solved for the in-plane shear modulus, G_{12}. It appears that the optimum fiber orientation, θ, for best strength results may not necessarily be the same as the optimum angle for best modulus results, but the 10° off-axis test seems to be a good compromise.

In addition to the previously mentioned Iosipescu test, there is at least one other test that is used for interlaminar shear. The reader is cautioned in advance, however, that although this other test is widely used as a screening test, the interlaminar strength data from this test should not be used for design purposes. The ASTM D2344/D2344M-00$^{\varepsilon 1}$ short-beam shear test [52] involves the use of a short beam loaded in three-point bending, as shown in figure 10.24. The resulting shear stress, τ_{xy}, due to the shear force, V, and the normal stress, σ_x, due to the bending moment, M, can be estimated by using well-known mechanics of materials formulas. While the shear stress is independent of specimen length, L, the normal stress, because of its dependence on the bending moment, is a linear function of L. Thus, failure by interlaminar shear can theoretically be induced by making the beam short enough so that under load, the shear stress will reach its limiting value before the normal stress does. This is why the test is referred to as the "short-beam shear test." However, Whitney [53,54] has used the theory of elasticity analyses of short-beam shear specimens to show that the actual state of stress in the vicinity of the applied load where failure initiates is much more complex than that

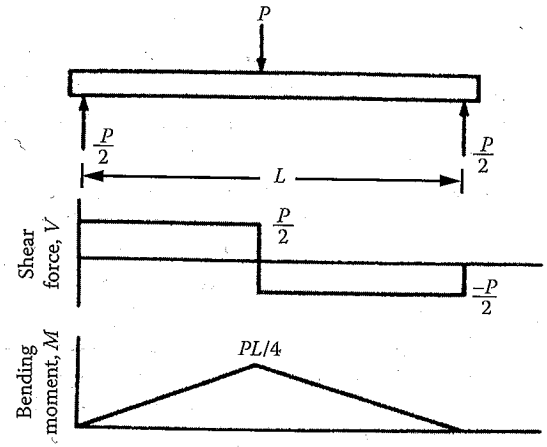

FIGURE 10.24
Short-beam shear test specimen with shear and moment diagrams.

predicted by the simple mechanics of materials formulas used in the D2344 standard. Thus, the interlaminar strength derived from the D2344 test is referred to only as "apparent" interlaminar shear strength and should not be used in design. According to D2344, such data can be used for quality control and specification purposes, however.

10.3.4 Flexure Tests

Recall from chapter 7 that unlike homogeneous, isotropic materials, composite laminates have flexural properties that are not necessarily the same as the corresponding tensile properties. Since many laminates are used as flexural members, there is a need to determine the flexural properties experimentally. The ASTM D790-03 test method [16], which was described in section 10.2.2, requires the use of beam specimens in three-point bending and can be used for both unreinforced plastics and high-modulus composites. Tables of recommended specimen dimensions are provided in the standard. It is important to realize, however, that in highly anisotropic composites such as unidirectional graphite/epoxy, through-thickness shear deformation can be significant unless the beam span-to-depth ratio is large enough. Thus, the specimen dimensions for these materials should be selected from the column corresponding to the highest span-to-depth ratio in the tables provided in D790-03. It is also important to remember from chapter 7 that the flexural modulus of highly anisotropic laminates depends on the ply-stacking sequence and is not necessarily the same as the in-plane Young's modulus of the laminate. According to Adams et al. [3], a new separate standard for flexural testing of composites is currently under development.

10.3.5 Interlaminar Fracture Tests

In section 9.4, the importance of interlaminar fracture was discussed, and the use of the strain energy release rate to characterize the interlaminar fracture toughness was described. The most important modes of delamination seem to be modes I and II, and the corresponding fracture toughnesses are usually characterized by the strain energy release rates G_{Ic} and G_{IIc}, respectively. Although a number of test methods for measuring G_{Ic} and G_{IIc} have been reported in the literature, the most widely used methods appear to be the double cantilever beam (DCB) test for G_{Ic} [fig. 9.17(a)] and the end-notched flexure (ENF) test for G_{IIc} [fig. 9.17(b)].

The calculation of G_{Ic} from experimental DCB data can be carried out by using the method of Whitney et al. [54,55], who analyzed each cracked half of the DCB specimen as though it were a cantilever beam (see fig. 9.17[a] and fig 10.25). Using the mechanics of materials beam theory, the tip deflection of the cantilever beam in figure 10.25 is

$$\frac{\delta}{2} = \frac{Pa^3}{3E_{fx}I} \tag{10.14}$$

where P is the applied load, a the beam length in figure 10.25 is the DCB crack length in figure 9.17(a), E_{fx} the flexural modulus of cracked half of DCB along the x direction, and I the moment of inertia of cracked half of DCB about centroidal axis of cracked half.

From equation (10.14), the compliance of the DCB specimen is found to be

$$s = \frac{\delta}{P} = \frac{64a^3}{E_{fx}th^3} \tag{10.15}$$

where t is the DCB specimen width (the crack width) and h = DCB specimen depth.

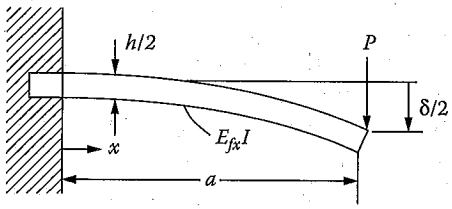

FIGURE 10.25
Cantilever beam representing half of the cracked DCB specimen.

The strain energy release rate, G_I, is then found by substituting equation (10.15) in equation (9.28) and differentiating with respect to the crack length, a. The result is

$$G_I = \frac{96P^2a^2}{E_{fx}t^2h^3} \tag{10.16}$$

or

$$G_I = \frac{3P\delta}{2ta} \tag{10.17}$$

where the deflection, δ, is given by equation (10.14). The critical strain energy release rate is then

$$G_{Ic} = \frac{96P_c^2a^2}{E_{fx}t^2h^3} \tag{10.18}$$

or

$$G_{Ic} = \frac{3P_c\delta_c}{2ta} \tag{10.19}$$

where P_c and δ_c are the critical values of the load and deflection, respectively, measured at the onset of crack growth. Whitney et al. [55] suggested that G_{Ic} could also be determined by rearranging equation (10.19) as

$$G_{Ic} = \frac{3H}{2t} \tag{10.20}$$

where $H = P_c\delta_c/a$ is a constant, and averaging H over some number of data points during continuous loading and crack extension. The average value of H is given by

$$H = \frac{1}{N}\sum_{i=1}^{N}\frac{P_{ci}\delta_{ci}}{a_i} \tag{10.21}$$

where P_{ci}, δ_{ci} are the critical values of P and δ, respectively, associated with the ith crack length a_i, and N the total number of data points

Several other data reduction schemes for the DCB test are reviewed by Whitney [54]. The relevant ASTM Standard for the DCB test is D5528-01 [56].

The determination of G_{IIc} from ENF test data can be accomplished by using the method of Russell and Street [57,58], who employed the elementary beam theory to derive the expression

$$G_{II} = \frac{9P^2a^2s}{2t(2L^3 + 3a^3)} \tag{10.22}$$

where the parameters P, a, t, and L are all defined in figure 9.17(b) and $s = \delta/P$ is the midspan compliance. The critical strain energy release rate, G_{IIc}, then corresponds to the critical load, P_c, and the associated compliance, s_c, at the onset of crack growth. The compliance, s, can be determined experimentally or calculated from the following equation, which was also derived using the elementary beam theory [57]:

$$s = \frac{(2L^3 + 3a^3)}{8E_{fx}th^3} \tag{10.23}$$

where E_{fx} is now the flexural modulus of the beam of depth $2h$, as shown in figure 9.17(b). Carlsson et al. [59] have used the Timoshenko beam theory to modify equation (10.22) and equation (10.23), so that the effects of shear deformation are included. Several other test methods for measurement of G_{Ic} and G_{IIc} are examined in detail by Whitney [54] and by Adams et al. [3].

Since the loading conditions in most composite structures are generally such that more than one fracture mode would result, the experimental investigations of mixed mode fracture are of considerable interest. In composite laminates, Mixed Mode I and Mode II interlaminar fracture is probably the most commonly occurring case of this type. The ASTM standard for mixed Mode I/Mode II interlaminar fracture is the mixed mode bending (MMB) test, D6671/D6671M-04$^{\varepsilon 1}$ [60], which involves a laminated beam specimen with a delamination starter crack on one end. The MMB test was originally developed at NASA by Reeder and Crews [61,62]. As shown in figure 10.26, the MMB test fixture is designed to produce pure Mode II delamination and measurement of the Mode II energy release rate, G_{II}, when the moment arm distance, c, is zero and the applied load P acts at specimen midspan. Then as the distance c is increased, and the applied load P moves away from midspan, the Mode I contribution and the mode mixity G_I/G_{II} increases accordingly. Thus, the MMB test is actually a combination of the DCB test for measuring G_I and

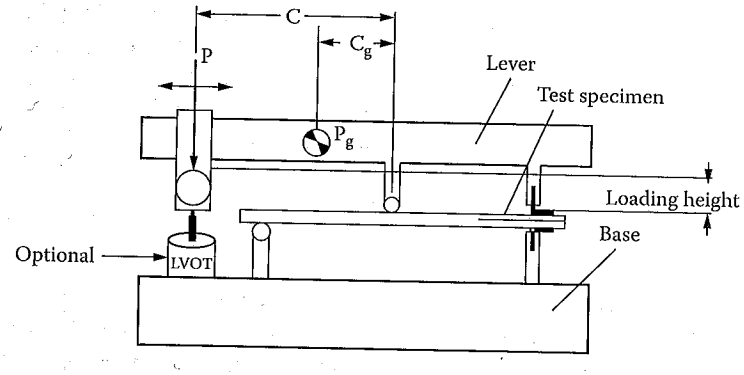

FIGURE 10.26
Test fixture for MMB test. (From ASTM Standard D6671/D6671M-04$^{\varepsilon 1}$. Copyright ASTM International. Reprinted with permission.)

the ENF test for measuring G_{II}, and by varying the distance c, various degrees of G_I/G_{II} mode mixity can be achieved. The MMB test has been modified for the measurement of mixed mode fracture in adhesively bonded joints by Liu et al. [63,64].

10.3.6 Fiber/Matrix Interface Tests

Good adhesion between the fiber and the matrix is a fundamental requirement if a composite is to be a useful structural material, and optimization of the fiber/matrix interface can only occur if reliable methods for measurement of fiber/matrix interfacial strength are available. One such method, a single-fiber fragmentation technique, has been developed and used by Drzal et al. [65–67]. The specimen, shown in figure 10.27, consists of a single fiber embedded in a dogbone tensile specimen of matrix resin. This specimen is loaded in tension under a microscope until

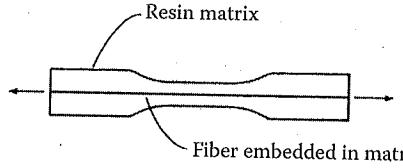

FIGURE 10.27
Single-fiber fragmentation specimen developed by Drzal et al. (From Drzal, L.T., Rich, M.J., and Lloyd, P.F. 1982. *Journal of Adhesion*, 16, 1–30.; Drzal, L.T., Rich, M.J., Koenig, M.F., and Lloyd, P.F. 1983. *Journal of Adhesion* 16, 133–152. With permission.)

the fiber breaks up into segments corresponding to the critical length, L_c, which are measured by using the microscope. If the fiber tensile strength, $S_{fl}^{(+)}$, corresponding to the critical length, and the fiber diameter, d, are known, then the interfacial shear strength can be estimated from equation (6.16), which is repeated here as equation (10.24).

$$\tau_y = \frac{d s_{fl}^{(+)}}{2L_c} \tag{10.24}$$

Since the observed lengths actually vary because of variations in fiber and matrix properties, a statistical distribution of fiber lengths must be used. If the measured values of L_c/d can be fitted by a two-parameter Weibull distribution, the mean value of interfacial shear strength can be expressed as [65]

$$\tau_y = \frac{S_{fl}^{(+)}}{2\beta}\Gamma\left(1-\frac{1}{\alpha}\right) \tag{10.25}$$

where Γ is the gamma function and α and β are the shape and scale parameters, respectively, for the two-parameter Weibull distribution.

In the so-called microbond test, single fiber is embedded in a resin droplet, and the free end of the fiber is loaded in tension until the fiber pulls out of the resin [68]. The interfacial strength is simply the pullout force divided by the interfacial area. One potential difficulty with this test is that it may be difficult to reproduce the composite resin matrix cure conditions in a small droplet of resin [68,69].

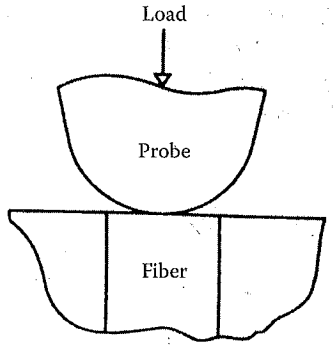

FIGURE 10.28
Microindenter test for fiber/matrix interfacial strength. (From Mandell, J.F., Grande, D.H., Tsiang, T.H., and McGarry, F.J. 1986. *Composite Materials: Testing and Design (Seventh Conference)*, ASTM STP 893, pp. 87–108. American Society for Testing and Materials, Philadelphia, PA. Copyright ASTM. Reprinted with permission.)

TABLE 10.2
Interfacial Shear Strength Values Obtained with Different Techniques

Fiber Type	Interfacial Shear Strength (MPa)		
	Fragmentation	Microbond	Microindentation
AS-4	68	50	71
AU-4	37	23	55
IM6-600	47	15	43
IM6-100	40	19	37
IM6-U	22	15	27

Source: From McDonough, W.G., Herrera-Franco, P.J., Wu, W.L., Drzal, L.T., and Hunston, D.L. 1991. In *Advanced Materials/Affordable Processes, Proceedings of 23rd International SAMPE Technical Conference*, Kiamesha Lake, NY, pp. 247–258. Society for Advancement of Material and Process Engineering, Covina, CA. Reprinted by permission of the Society for the Advancement of Material and Process Engineering.

While a single-fiber specimen is required for the two techniques described above, in situ fiber/matrix interfacial shear strength in composite specimens may be measured by using the microindentation technique [69,70]. As shown in figure 10.28, this approach involves the use of a diamond microindenter to load the end of a fiber in longitudinal compression until debonding between the fiber and the matrix occurs. The experimental data for debonding load are combined with a finite element analysis in order to calculate the interfacial strength.

A comparison of the three interfacial strength measurement techniques described above has been reported by McDonough et al. [68], and the results for carbon fibers having different surface treatments and the same epoxy matrix are shown in table 10.2. It was concluded that while the single-fiber fragmentation technique and the microindentation techniques showed good agreement, the microbond technique produced interfacial strength values that were consistently lower than those of the other two methods. The above-mentioned uncertainty regarding the state of cure in the microbond droplet was given as the reason for these results.

10.4 Measurement of Viscoelastic and Dynamic Properties

In chapter 8, creep, relaxation, damping, and strain rate dependence were described as four important physical manifestations of viscoelastic behavior. All these characteristics can be determined experimentally, but in this section we will only describe test methods for the measurement of creep compliance and damping. Since the complex modulus notation

conveniently describes both dynamic stiffness and damping of linear viscoelastic materials, vibration test methods for the measurement of the complex moduli of composites will be considered. The use of vibration tests of beams and plates to determine dynamic elastic moduli alone will also be reviewed. Wave propagation test methods will not be covered here.

10.4.1 Creep Tests

A creep test usually consists of the application of constant loading to a specimen, followed by measurement of the resulting time-dependent strains in the specimen, as shown schematically in figure 8.1(a). Although there are no standard creep test methods for composites at this time, creep test methods and creep rupture test methods have been standardized for tensile, compressive, and flexural creep of plastics [71] and flexure creep of sandwich beams [72]. For example, the apparatus for flexure creep testing of sandwich beams is shown in figure 10.29 from ref. [72]. Through a mechanical lever arrangement, a constant load is applied at midspan of the simply supported sandwich beam, and midspan creep deflection is measured as a function of time. In a creep rupture test (or stress rupture test), the time to failure is measured rather than the time-dependent strain or deflection in the specimen.

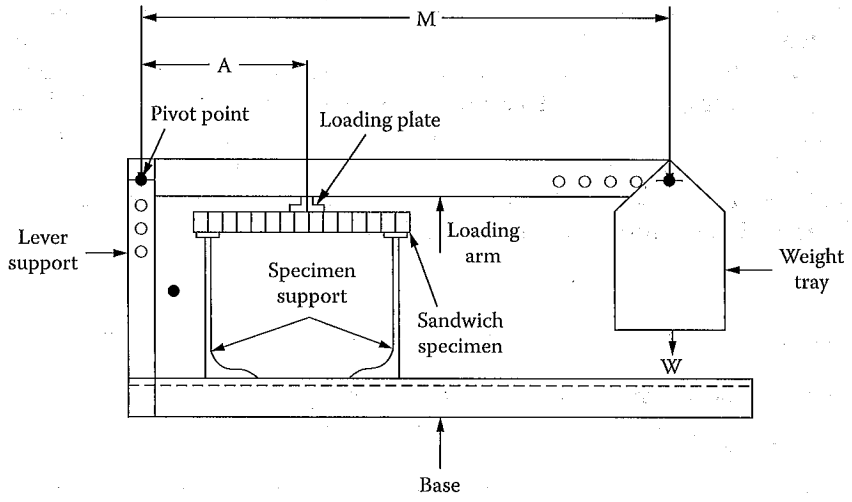

FIGURE 10.29
Test apparatus for measurement of flexure creep of sandwich beams. (From ASTM Standard C 480-99 [Reapproved 2005]. Copyright ASTM International. Reprinted with permission.)

In principle, any of the previously described composite test methods can be used to characterize creep if the following provisions are made:

1. The applied loading on the specimen should be constant.
2. The resulting strains or deflections in the specimen should be measured as a function of elapsed time under load.
3. The specimen should be kept under controlled environmental conditions for the duration of the test.

Since viscoelastic behavior depends on temperature and humidity, the specimen would normally be enclosed in an environmental chamber. Stability of the measurement system electronics over long periods of time is also very important.

As shown by Halpin and Pagano [73] ,the principal creep compliances $S_{11}(t)$, $S_{22}(t)$, $S_{12}(t) = S_{21}(t)$, and $S_{66}(t)$ for a linear viscoelastic, orthotropic lamina can be determined by conducting the three tensile creep tests in figure 10.30. For example, in the creep test of the longitudinal specimen in figure 10.30(a) the constant stress, σ_1, is applied; the time-dependent longitudinal strain, $\varepsilon_1(t)$, and the transverse strain, $\varepsilon_2(t)$, are measured, and the longitudinal creep compliance is determined from the equation

$$S_{11}(t) = \frac{\varepsilon_1(t)}{\sigma_1} \tag{10.26}$$

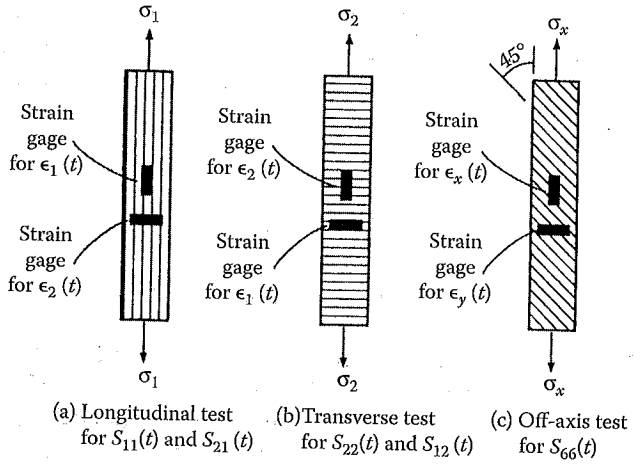

FIGURE 10.30
Tensile tests for measurement of creep compliances of an orthotropic viscoelastic lamina.

whereas

$$S_{21}(t) = \frac{\varepsilon_2(t)}{\sigma_1} \tag{10.27}$$

For the transverse tensile creep test in figure 10.30(b), the constant transverse stress, σ_2, is applied, and the resulting strains are used to find the creep compliances

$$S_{22}(t) = \frac{\varepsilon_2(t)}{\sigma_2} \tag{10.28}$$

and

$$S_{12}(t) = \frac{\varepsilon_1(t)}{\sigma_2} \tag{10.29}$$

The data of Halpin and Pagano [73] and γ others from such tests have shown that $S_{12}(t) = S_{21}(t)$.

Finally, the off-axis tensile creep test in figure 10.30(c) can be used to determine the shear creep compliance $S_{66}(t)$. For example, if the constant uniaxial stress is σ_x and the fiber orientation $\theta = 45°$, a transformation of stresses gives the shear stress along the principal material axes as $\tau_{12} = \sigma_x/2$. The corresponding time-dependent shear strain, $\gamma_{12}(t)$, can be determined from the measured strains, $\varepsilon_x(t)$ and $\varepsilon_y(t)$, by modifying equation (10.13) as $|\gamma_{12}(t)| = |\varepsilon_x(t)| - |\varepsilon_y(t)|$. In practice, a more accurate determination of the shear strain $\gamma_{12}(t)$ is possible by using a strain gage rosette that has three strain gages oriented at 45° to each other [74]. The shear compliance is given by

$$S_{66}(t) = \frac{\gamma_{12}(t)}{\tau_{12}} \tag{10.30}$$

Similar tensile creep tests of composites have been reported by Beckwith [75,76] and Sullivan (ref. [30] of chap. 8).

Uniaxial compressive creep testing presents the same difficulties that were discussed earlier in section 10.3.2, and there appear to be few references dealing with such tests. For example, Irion and Adams [77] have used the Wyoming-modified Celanese fixture [27] for compressive creep testing of unidirectional composites.

Since viscoelastic behavior is dependent on the stress-time history, preconditioning of creep specimens is recommended. Lou and Schapery [78] have suggested that mechanical conditioning of specimens before creep testing leads to much more repeatable test results. Specimens are mechanically conditioned by subjecting them to specified numbers of cycles of creep and recovery (loading and unloading) at a certain stress level. The actual creep tests are then conducted at stresses less than or equal to the conditioning stress. In creep tests of polymer composites where the effects of physical aging are being studied, rejuvenation of the specimens at temperatures above T_g is necessary before the aging and/or creep tests begin (ref. [30] of chap. 8).

In the discussion of viscoelastic behavior in chapter 8, linear viscoelastic behavior was assumed. Experiments have shown, however, that polymer composites may exhibit nonlinear viscoelastic behavior at relatively low stress levels [75,78]. For example, Beckwith [75,76] has shown that the creep compliances for filament-wound S-glass/epoxy composites at various lay-ups followed a power law of the form

$$S(t) = S_0 + S_1 t^n \tag{10.31}$$

where $S(t)$ is the creep compliance, S_0 the initial elastic compliance, and S_1 and n the empirically determined parameters.

The exponent, n, was found to be approximately equal to 0.19 for all compliances in the linear range, but at high stress levels and after multiple cycles of loading and unloading microcracking in the materials caused the exponent n to increase substantially.

Recall from chapter 8 that for a linear viscoelastic material, the time domain creep compliance is related to the frequency domain complex compliance by a Fourier transform pair, as are the relaxation modulus and the complex modulus. This relationship makes it possible to obtain time domain creep and relaxation characteristics from frequency domain test data and vice versa. Using frequency domain complex modulus data and the Fourier transform approach, Gibson et al. [79,80] have developed alternative techniques for determination of creep and relaxation behavior of linear viscoelastic composites in both tension and compression. A similar technique [81] involves using frequency domain vibration tests to determine the parameters in a spring-dashpot model (recall section 8.2.2), and then substituting those same spring-dashpot parameters in the corresponding time domain creep compliance expression. Vibration test techniques for measurement of complex moduli will be discussed in the next section.

Finally, it is important to remember that, for polymer matrix composites, the viscoelastic behavior of the composite is dominated by the viscoelastic behavior of the polymer matrix material. So, for example, if it is not feasible or desirable to conduct creep tests of the

structure, a viable alternative is to conduct creep tests of the neat resin polymer matrix material and then use micromechanical or macromechanical models to predict the corresponding creep behavior of the composite material or structure. Examples of such an approach involving the use of quasielastic analysis and the elastic–viscoelastic correspondence principle are given in section 8.2.3 and section 8.2.5, respectively. However, since linear viscoelastic behavior is the underlying assumption of both quasielastic analysis and the elastic–viscoelastic correspondence principle, the use of this approach must be supported by experimental evidence of linear viscoelastic behavior of the polymer matrix material, as discussed in section 8.2.

10.4.2 Vibration Tests

The complex modulus notation, which is convenient for the characterization of dynamic behavior of linear viscoelastic composites, was developed in chapter 8. The two components of the complex modulus (stiffness and damping) of a material are generally referred to as its dynamic mechanical properties, and measurement of these properties is often referred to as dynamic mechanical analysis. Dynamic mechanical properties may be measured by using either wave propagation or vibration experiments, but only vibration test methods will be discussed here.

The only relevant ASTM standards are D4065–01 [82], which was developed for unreinforced plastics, and E756–05 [83], which was developed for add-on surface damping treatments. In principle, some of the techniques described in these standards can also be used for composites. In practice, however, there are many pitfalls that must be avoided. For example, most commercially available dynamic mechanical testing machines or dynamic mechanical analyzers were developed for testing small specimens of unreinforced low modulus polymers, and the stiffness of the specimen mounting hardware in the machines is generally insufficient for use with high-modulus composites. To reduce the composite specimen stiffness to the range required for valid data with these devices, it may be necessary to use specimen thicknesses on the order of the single ply thickness, so that testing of multi-ply laminates may not be possible. In addition, the equations used for data reduction in these machines typically do not take into account coupling effects, transverse shear effects, and other peculiarities of composite material behavior. Valid dynamic mechanical property measurements are difficult to obtain, particularly with composite materials. Only a brief overview of test methods and difficulties will be given here, as a detailed review has been published elsewhere [84].

The complex modulus (recall eq. [8.75]) for a particular vibration test specimen is obtained by measuring the storage modulus and the loss factor of the specimen as it vibrates in the desired mode. Specimens usually consist

of rods, beams, or plates supported in such a way so as to minimize the extraneous damping due to the apparatus or the environment. Friction damping at specimen support points and transducer attachments, aerodynamic drag on the vibrating specimen, and phase lag in the instrumentation may all lead to erroneous damping data. Cross-verification of damping measurements using several different techniques is always a good way to locate potential problems.

The storage modulus is generally obtained by measuring a natural frequency of the specimen and by solving frequency equation for the specimen. For example, equation (8.111) can be used to solve for the longitudinal modulus of a composite bar if the frequency, f_n, for the nth mode, the specimen length, L, and the density, ρ, are measured. Similarly, equation (8.122) can be used to determine the flexural modulus, E_f, of a composite beam specimen [85]. Care must be taken to make sure that the effective modulus criteria have been met and that various effects such as coupling and transverse shear have been accounted for where necessary. As mentioned in section 8.3.2, transverse shear effects are much more significant for high-modulus composites than they are for conventional materials, and Timoshenko beam theory may be required for valid results. Figure 10.31 shows correction factors, which, when multiplied by modulus values from

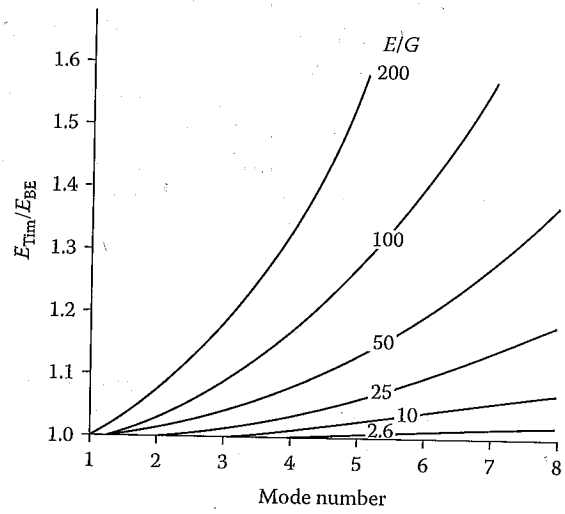

FIGURE 10.31
Correction factors required to correct modulus values from resonant frequency measurements using the Bernoulli–Euler theory to values using the Timoshenko beam theory. Factors are plotted as a function of mode number for several values of E/G and length/thickness ratio of 100. (From Dudek, T.J. 1970. *Journal of Composite Materials*, 4, 232–241. With permission.)

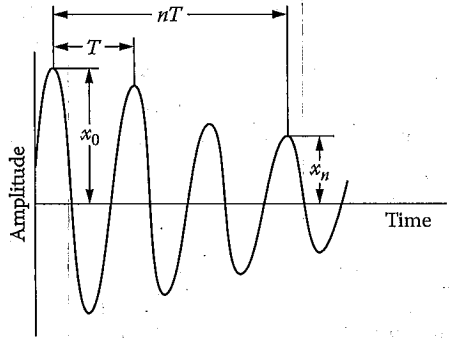

FIGURE 10.32
Free vibration decay curve for logarithmic decrement measurement.

the Bernoulli–Euler beam theory, yield corrected modulus values that are consistent with Timoshenko beam theory [86].

Damping is conveniently characterized by using the loss factor in the complex modulus notation. For lightly damped systems, the loss factor is related to the parameters that are used to characterize damping in a single-degree-of-freedom (SDOF) spring-mass system. The SDOF-damping parameters are typically estimated by curve fitting to the measured response of specimens in either free vibration or forced vibration if a single mode can be isolated for the analysis.

In the free vibration experiment, a specimen such as a rod or a beam is released from some initial displacement, or a steady-state excitation is removed, and the ensuing free vibration decay of the specimen is observed (fig. 10.32). The logarithmic decrement, Δ, is calculated from such a decay curve by using the equation

$$\Delta = \frac{1}{n} \ln \frac{x_0}{x_n} \tag{10.32}$$

where x_0 and x_n are amplitudes measured n cycles apart, as shown in figure 10.32. Equation (10.32) is based on the assumption of viscous damping, but for light damping, the loss factor, η, is related to the logarithmic decrement by [87]

$$\eta = \frac{\Delta}{\pi} \tag{10.33}$$

Care must be taken to ensure that only one mode of vibration is present in the response decay curve, as the damping value should be measured for one particular mode.

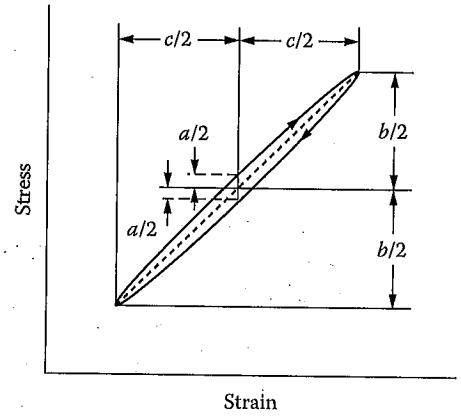

FIGURE 10.33
Hysteresis loop from fixed frequency forced oscillation test.

One type of forced vibration test method involves fixed frequency oscillation of the specimen in a testing machine and simultaneous plotting of the resulting stress–strain hysteresis loop (fig. 10.33). Using the dimensions a, b, and c from such hysteresis loops at a frequency, f, the components of the complex modulus can then be estimated by the equations [84]

$$\eta(f) = \frac{a}{b} \tag{10.34}$$

and

$$E'(f) = \frac{b}{c} \tag{10.35}$$

Another forced vibration technique is based on variation of the excitation frequency, simultaneous measurement of the response, and plotting of the magnitude and/or phase of the response in the frequency domain. The resulting frequency response curve, or frequency response spectrum (fig. 10.34), has a number of peaks that represent natural frequencies of the specimen, and SDOF curve-fitting techniques can be applied to these peaks to extract the data needed to compute the complex modulus. The

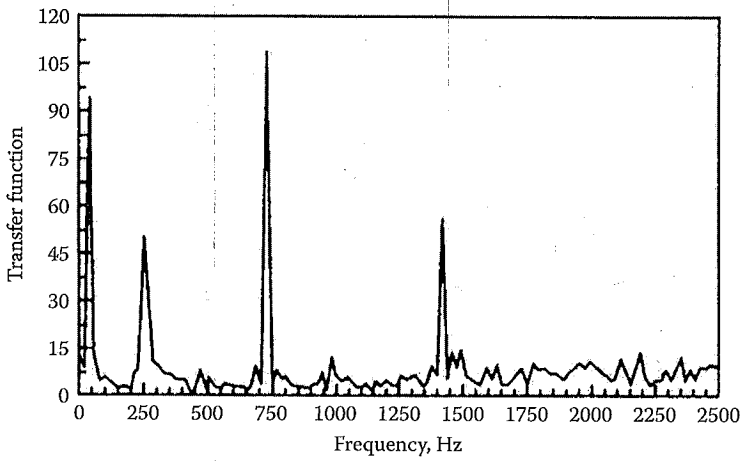

FIGURE 10.34
Typical specimen transfer function vs. frequency, or frequency response curve.

previously. The loss factor may be determined by using the half power bandwidth equation

$$\eta = \frac{\Delta f}{f_n} \tag{10.36}$$

where Δf is the bandwidth at the half power points on the peak and f_n the peak frequency for the nth mode of vibration

Digital frequency spectrum analyzers or Fast Fourier transform (FFT) analyzers are commonly used for this purpose. In recent years, virtual instrument software running on personal computers has become a popular alternative to dedicated spectrum analyzer instruments. Excitation may be variable frequency sinusoidal, random, or impulsive. The impulse–frequency response method is perhaps the fastest and simplest method in this category [85,88,89]. A cantilever beam test apparatus based on the impulse–frequency response method is shown in figure 10.35. In this apparatus the beam specimen is impulsively excited by a hammer that has a small force transducer in its tip, while the specimen response is monitored by a noncontacting displacement sensor. Excitation and response signals are fed into the FFT analyzer, which computes and displays the frequency response function in real time. Curve fitting to the frequency response curve and calculation of the complex modulus are accomplished by a desktop computer that is interfaced with the FFT analyzer. Frequency dependence of the complex moduli can be determined by testing beams of different lengths and/or by taking data for multiple modes of vibration. The experimental

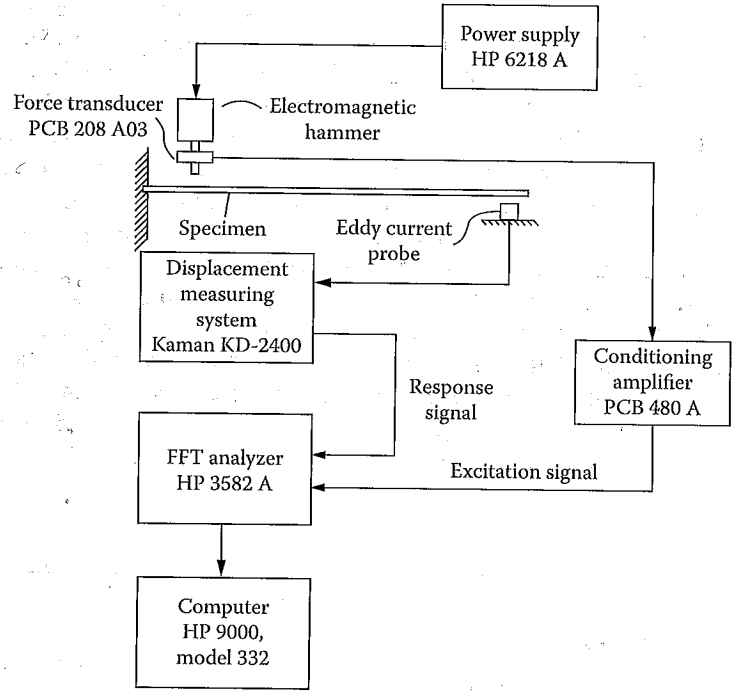

FIGURE 10.35
Cantilever beam test apparatus for impulse–frequency response method.

Impulse techniques have also been used in conjunction with laminated plate vibration models to determine the elastic constants of composite plates [90,91]. An impulse test apparatus based on this method has been developed for measurement of the complex extensional modulus of reinforcing fibers at elevated temperatures [92,93]. Damping has been found to be particularly sensitive to damage and degradation in composites, and the impulse-frequency response method has been successfully used in such studies [94,95].

In recent years, the use of modal vibration measurements to determine dynamic mechanical properties of composite materials and their constituents has been extended to numerous nontraditional applications such as determination of global elastic constants of composites, the distribution of reinforcing fibers within composites, time–domain creep response of composites, elevated-temperature behavior of composites and their constituents, interlaminar fracture toughness of composites, and the presence of

of modal vibration response have been extended to the micromechanical and nanomechanical levels. For example, microscanning laser vibrometry has been used to investigate the modal vibration response of composite microelectromechanical systems such as microlayered ultrasonic sensors [97], and measured modal frequencies of cantilevered carbon nanotubes have been used in a combined experimental and numerical approach to indirectly determine the elastic modulus of the nanotubes [98].

In conclusion, dynamic test methods provide rapid and inexpensive alternatives to conventional static test methods in the measurement of composite stiffnesses. The dynamic test also yields information on the internal damping of the material, which is not only an important design property, but also a useful nondestructive test parameter that can be related to the integrity of the material. It is conceivable that such test methods could be integrated into the manufacturing process itself in order to provide on-line monitoring and control of composite material properties.

10.5 Problems

1. Derive equation (10.2).
2. The results of longitudinal, transverse, and 45° off-axis tensile tests on samples from an orthotropic lamina are shown in figure 10.36. Based on these results, find numerical values for the engineering constants E_1, E_2, υ_{12}, and G_{12}.

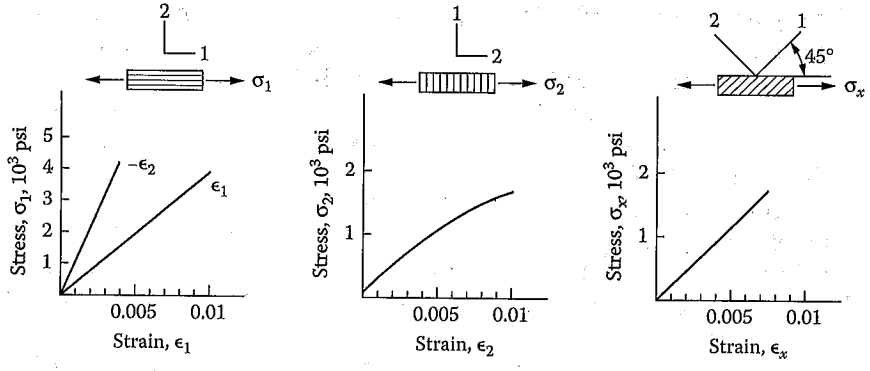

FIGURE 10.36

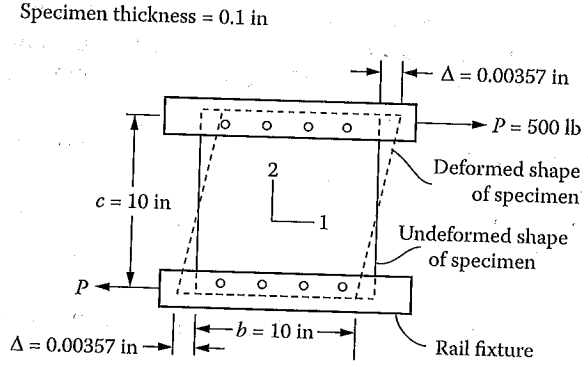

FIGURE 10.37
Shear deformation of a carbon/epoxy specimen during a rail shear test.

3. The in-plane shear modulus, G_{12}, of a carbon/epoxy lamina is to be measured by using the rail shear test shown in figure 10.37. The test is conducted on a 10 in × 10 in × 0.1 in (254 mm × 254 mm × 2.54 mm) panel specimen, which deforms under the applied load as shown. Determine the value of G_{12} from these data.
4. The 45° off-axis test shown in figure 10.38 is conducted on a 10 in × 1 in × 0.1 in (254 mm × 25.4 mm × 2.54 mm) carbon/epoxy specimen, which deforms as shown under the applied load. It is also known from separate tensile tests that $E_1 = 32 \times 10^6$ psi (220 GPa), $E_2 = 1.0 \times 10^6$ psi (6.89 GPa), and $\upsilon_{12} = 0.3$. Determine the value of G_{12} from these test data.
5. A 45° off-axis specimen cut from an AS/3501 carbon/epoxy lamina is subjected to a tensile test. The specimen is 3 mm thick and 25 mm wide, and a tensile load of $F_x = 1$ kN on the specimen produces a corresponding strain $\varepsilon_x = 0.0003$. It is claimed that the off-axis Young's modulus, E_x, can be determined from these results. Is this a valid claim? If so, why? If not, why not?

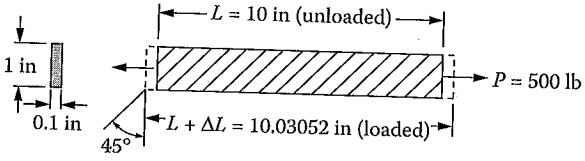

6. Describe the measurements that must be taken and the equations that must be used to determine the shear creep compliance, $S_{66}(t)$, of a unidirectional viscoelastic lamina by using a rail shear test.
7. Extensional vibration experiments are conducted on longitudinal, transverse, and 45° off-axis unidirectional composite specimens, and the complex moduli results for a particular vibration frequency are, respectively:

$$E_1^* = E_1'(1+i\eta_1) = 35.6(1+0.004i)\text{GPa}, \quad \text{for } \theta = 0°$$

$$E_2^* = E_2'(1+i\eta_2) = 10.8(1+0.009i)\text{GPa}, \quad \text{for } \theta = 90°$$

$$E_x^* = E_x'(1+i\eta_x) = 11.6(1+0.011i)\text{GPa}, \quad \text{for } \theta = 45°$$

   Using the above data derive the equations for both parts of the complex shear modulus, $G_{12}^* = G_{12}'(1+i\eta_{12})$, then find numerical values for both parts. Assume that all loss factors are very small (<<1), and that the major Poisson's ratio $v_{12} = 0.3$ is a real constant.
8. Using the results from Problem 7, derive the equations for both parts of the off-axis complex modulus, $E_x^* = E_x'(1+i\eta_x)$ E, for an arbitrary angle θ; then find numerical values of both parts for an angle of θ = 30°.
9. Describe an experiment, and give the necessary equations for measurement of the complex flexural modulus, E_{fx}^*, of a symmetric laminated beam.
10. Describe an experiment, and give the necessary equations for the measurement of the complex extensional (or longitudinal) modulus, E_x^*, of a symmetric laminated bar.
11. Describe an experiment, and give the necessary equations for the measurement of the complex through-thickness shear modulus, G_{23}^*, of a unidirectional, specially orthotropic, transversely isotropic beam.
12. Describe an experiment, and give the necessary equations for measurement of the complex Young's modulus, E_m^*, of an isotropic matrix material.
13. Describe an experiment, and give the necessary equations for the measurement of the complex longitudinal modulus, E_{f1}^*, of a reinforcing fiber.
14. Describe an experiment, and give the necessary equations for

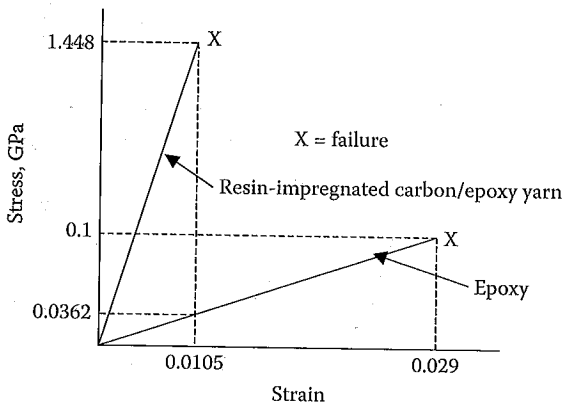

FIGURE 10.39
Stress–strain curves for epoxy and resin-impregnated carbon/epoxy yarn, for problem 15.

15. In order to determine the tensile Young's modulus and tensile strength of carbon fibers, a tensile test of a resin-impregnated carbon/epoxy yarn having a fiber volume fraction of 0.6 is conducted. A separate tensile test is conducted on the neat resin epoxy matrix material, and both stress-strain curves are shown in figure 10.39. Using these two stress–strain curves and micromechanics models, determine the fiber tensile Young's modulus, E_{f1}, and the fiber tensile strength, $s_{f1}^{(+)}$.
16. A 45° off-axis rail shear test specimen of an orthotropic lamina is shown in figure 10.40. Attached to the specimen are three strain gages that measure the normal strains ε_x, ε_y and ε_1 along the x, y, and 1 directions, respectively. The specimen thickness t = 0.1 inch

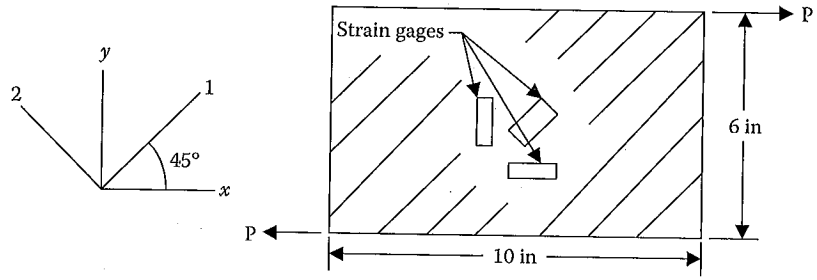

and the length and width are shown in figure 10.40. The applied shear load along the x direction is P = 500 lb, while the three measured strains are $\varepsilon_x = 0.00056$, $\varepsilon_y = 0.00075$, and $\varepsilon_1 = 0.00078$. Answer the following questions, giving both numerical values and units where appropriate. (a) Is it possible to determine the off-axis shear modulus G_{xy} from this data? If not, why not? If so, calculate G_{xy}. (b) Is it possible to determine the Poisson's ratio υ_{xy} from this data? If not, why not? If so, calculate υ_{xy}. (c) Is it possible to determine the shear-coupling ratio $\eta_{xy,x}$ from this data? If not, why not? If so, calculate $\eta_{xy,x}$. (d) Is it possible to determine the material shear strength S_{LT} from this data? If not, why not? If so, calculate S_{LT}. Hint: equation 10.10 is based on the assumption that the x,y axes are the same as the principal material axes 1,2 so that $\varepsilon_x = \varepsilon_1 = \varepsilon_y = \varepsilon_2 = 0$, but in this case the 1,2 axes are oriented at $\theta = 45^\circ$ from the x,y axes and equation 10.10 is not valid here.

17. The specimen geometry and the frequency response curve for the second mode flexural vibration of a laminated composite cantilever beam specimen is shown in figure 10.41. The specimen has length L = 8.913 in, width w = 0.756 in, thickness t = 0.04 in, and specific weight of $\gamma = 0.064$ lb/in^3 (note: $\gamma = \rho g$, where ρ = density

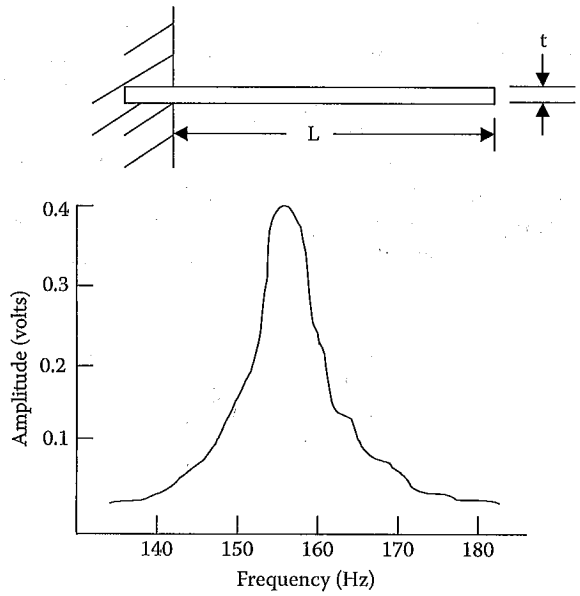

FIGURE 10.41

and g = gravitational acceleration = 386 in/s^2). The specimen is clamped across the width as shown. Based on this data, give your best estimates for the following properties of the specimen, (a) the flexural modulus, E_f, and (b) the flexural loss factor, η_f.

References

1. *ASTM Standards 2005*, vol. 15.03, *Space Simulation; Aerospace and Aircraft; Composite Materials*. ASTM International, West Conshohocken, PA.
2. *ASTM Standards 2005*. vol. 15.01, *Refractories; Activated Carbon; Advanced Ceramics*. ASTM International, West Conshohocken, PA.
3. Adams, D.F., Carlsson, L.A., and Pipes, R.B. 2003. *Experimental Characterization of Advanced Composite Materials*, 3rd ed. CRC Press, Boca Raton, FL.
4. Jenkins, C.H., ed. 1998. *Manual on Experimental Methods of Mechanical Testing of Composites*, 2d ed. Society for Experimental Mechanics, Bethel, CT.
5. D4762-04 2005. *Standard Guide for Testing Polymer Matrix Composite Materials*, vol. 15.03, *Space Simulation; Aerospace and Aircraft; Composite Materials*. ASTM International, West Conshohocken, PA.
6. C 1557.03$^{\varepsilon 1}$ 2005. *Standard Test Method for Tensile Strength and Young's Modulus of Fibers*, vol. 15.01, *Refractories; Activated Carbon; Advanced Ceramics*. ASTM International, West Conshohocken, PA.
7. McMahon, P.E. 1973. *Graphite Fiber Tensile Property Evaluation, Analysis of Test Methods for High Modulus Fibers and Composites*, ASTM STP 521, pp. 367–389. ASTM International, West Conshohocken, PA.
8. D4018-99 2005. *Standard Test Methods for Properties of Continuous Filament Carbon and Graphite Fiber Tows*, vol. 15.03, *Space Simulation; Aerospace and Aircraft; Composite Materials*. ASTM International, West Conshohocken, PA.
9. Tsai, C.- L. and Daniel, I.M. 1994. Method for thermo-mechanical characterization of single fibers. *Composites Science and Technology*, 50, 7–12.
10. Kawabata, S. 1989. Measurements of anisotropic mechanical property and thermal conductivity of single fiber for several high performance fibers, in Vinson, J.R. ed., *Proceedings of the 4th Japan–U.S. Conference on Composite Materials*, pp. 253–262. CRC Press, Boca Raton, FL.
11. Tsai, C. – L. and Daniel, I.M. 1999. Determination of shear modulus of single fibers. *Experimental Mechanics*, 39(4), 284–286.
12. D638-03. 2005. *Standard Test Method for Tensile Properties of Plastics*, vol. 08.01, *Plastics*. ASTM International, West Conshohocken, PA.
13. D618-05. 2005. *Standard Practice for Conditioning Plastics for Testing*, vol. 08.01, *Plastics*. ASTM International, West Conshohocken, PA.
14. D695-02a. 2005. *Standard Test Method for Compressive Properties of Rigid Plastics*, vol. 08.01, *Plastics*. ASTM International, West Conshohocken, PA.
15. Novak, R.C. and Bert, C.W. 1968. Theoretical and experimental bases for

16. D790-03 2005. *Standard Test Methods for Flexural Properties of Unreinforced and Reinforced Plastics and Electrical Insulating Materials*, vol. 08.01, *Plastics*. ASTM International, West Conshohocken, PA.
17. D3171-99 (Reapproved 2004), *Standard Test Methods for Constituent Content of Composite Materials*, vol. 15.03, *Space Simulation; Aerospace and Aircraft; Composite Materials*. ASTM International, West Conshohocken, PA (2005).
18. D3039/D3039M-00$^{\varepsilon 2}$ 2005. *Standard Test Method for Tensile Properties of Polymer Matrix Composite Materials*, vol. 15.03, *Space Simulation; Aerospace and Aircraft; Composite Materials*. ASTM International, West Conshohocken, PA.
19. Carlsson, L.A. and Pipes, R.B. 1989. *Experimental Characterization of Advanced Composite Materials*. Prentice-Hall, Inc., Englewood Cliffs, NJ.
20. Pagano, N.J. and Halpin, J.C 1968. Influence of end constraint in the testing of anisotropic bodies. *Journal of Composite Materials*, 2, 18–31.
21. Jones, R.M. 1975. *Mechanics of Composite Materials*. Hemisphere Publishing Co., New York.
22. Horgan, C.O. 1972. Some remarks on Saint-Venant's principle for transversely isotropic composites. *Journal of Elasticity*, 2(4), 335–339.
23. Choi, I. and Horgan, C.O. 1977. Saint-Venant's principle and end effects in anisotropic elasticity. *Journal of Applied Mechanics*, 44, 424–430.
24. Horgan, C.O. 1982. Saint-Venant end effects in composites. *Journal of Composite Materials*, 16, 411–422.
25. Rawlinson, R.A. 1991. The use of crossply and angleply composite test specimens to generate improved material property data, *How concept becomes reality, Proceedings of the 36th International SAMPE Symposium and Exhibition*, 36, Book 1, pp. 1058–1068. Society for the Advancement of Material and Process Engineering, Covina, CA.
26. Hart-Smith, L.J. 1992. Backing out equivalent unidirectional lamina strengths from tests on cross-plied laminates, in *Materials. Working for You in the 21st Century. Proceedings of the 37th International SAMPE Symposium and Exhibition*, 37, pp. 977–990. Society for the Advancement of Material and Process Engineering, Covina, CA.
27. Berg, J.S. and Adams, D.F. 1989. An evaluation of composite material compression test methods. *Journal of Composites Technology and Research*, 11(2), 41–46.
28. Schoeppner, G.A. and Sierakowski, R.L. 1990. A review of compression test methods for organic matrix composites. *Journal of Composites Technology and Research* 12(1), 3–12.
29. Welsh, J.R. and Adams, D.F. 1997. Current status of compression test methods for composite materials. *SAMPE Journal*, 33(1), 35–43.
30. Odom, E.M. and Adams, D.F 1990. Failure modes of unidirectional carbon/epoxy composite compression specimens. *Composites*, 21(4), 289–296.
31. Budiansky, B. and Fleck, N.A. 1993. Compressive failure of fibre composites. *Journal of the Mechanics and Physics of Solids*, 41(1), 183–211.
32. D3410/D3410M – 03, *Standard Test Method for Compressive Properties of Polymer Matrix Composite Materials with Unsupported Gage Section by Shear Loading*, vol. 15.03, *Space Simulation; Aerospace and Aircraft; Composite Materials*. ASTM International, West Conshohocken, PA (2005).

33. D5467/D5467M-97 (Reapproved 2004), *Standard Test Method for Compressive Properties of Unidirectional Polymer Matrix Composite Materials using a Sandwich Beam*, vol. 15.03, *Space Simulation; Aerospace and Aircraft; Composite Materials*. ASTM International, West Conshohocken, PA (2005).
34. D6641/D6641M - 01$^{\varepsilon 1}$, *Standard Test Method for Determining Compressive Properties of Laminated Polymer Matrix Composite Materials using a Combined Loading Compression (CLC) Test Fixture*, vol. 15.03, *Space Simulation; Aerospace and Aircraft; Composite Materials*. ASTM International, West Conshohocken, PA (2005).
35. Adsit, N.R. 1983. Compression testing of graphite/epoxy, in Chait, R. and Papirno, R. eds., *Compression Testing of Homogeneous Materials*, ASTM STP 808, pp. 175–186. American Society for Testing and Materials, Philadelphia, PA.
36. Crasto, A.S. and Kim, R.Y. 1991. Compression strength of advanced composites from a novel mini-sandwich beam. *SAMPE Quarterly*, 22(3), 29–39.
37. Wilson, D.W., Altstadt, V., and Prandy, J. 1992. On the use of laminate test methods to characterize lamina compression strength, in *Materials Working for You in the 21st Century, Proceedings of the 37th International SAMPE Symposium and Exhibition*, 37, pp. 606–619. Society for the Advancement of Material and Process Engineering, Covina, CA.
38. Boeing Specification Support Standard BSS 7260, *Advanced Composite Tests*. The Boeing Company, Seattle, WA, issued 1982, rev. 1988.
39. Nettles, A.T. and Hodge, A.J. 1991. Compression after impact testing of thin composite materials, in *Advanced materials/affordable processes, Proceedings of the 23rd International SAMPE Technical Conference*, 23, pp. 177–183. Society for the Advancement of Material and Process Engineering, Covina, CA.
40. D7137/D7137M-05$^{\varepsilon 1}$, 2005. *Standard Test Method for Compressive Residual Strength Properties of Damaged Polymer Matrix Composite Plates*, vol. 15.03, *Space Simulation; Aerospace and Aircraft; Composite Materials*. ASTM International, West Conshohocken, PA.
41. Adams, D.F. 2005. A comparison of shear test methods. *High Performance Composites*, 13(5), 9–10.
42. D5379/D5379M, 2005. *Standard Test Method for Shear Properties of Composite Materials by the V-notched Beam Test Method*, vol. 15.03, *Space Simulation; Aerospace and Aircraft; Composite Materials*. ASTM International, West Conshohocken, PA.
43. D7078/D7078M-05, 2005. *Standard Test Method for Shear Properties of Composite Materials by the V-notched Rail Shear Test Method*, vol. 15.03, *Space Simulation; Aerospace and Aircraft; Composite Materials*. ASTM International, West Conshohocken, PA.
44. Iosipescu, N. 1967. New accurate procedure for single shear testing of metals. *Journal of Materials*, 2(3), 537–566.
45. Walrath, D.E. and Adams, D.F. 1983. The Iosipescu shear test as applied to composite materials. *Experimental Mechanics*, 23(1), 105–110.
46. Adams, D.F. and Walrath, D.E. 1987. Current status of the Iosipescu shear

47. Adams, D.F. and Walrath, D.E. 1987. Further development of the Iosipescu shear test method. *Experimental Mechanics*, 27(2), 113–119.
48. Adams, D.F. 1990. The Iosipescu shear test method as used for testing polymers and composite materials. *Polymer Composites*, 11(5), 286–290.
49. Lee, S. and Munro, M. 1986. Evaluation of in-plane shear test methods for advanced composite materials by the decision analysis technique. *Composites*, 17(1), 13–22.
50. D4255/D4255M-01, 2005. *Standard Test Method for In-plane Shear Properties of Polymer Matrix Composite Materials by the Rail Shear Method*, vol. 15.03, *Space Simulation; Aerospace and Aircraft; Composite Materials*. ASTM International, West Conshohocken, PA.
51. D3518/D3518M-94 (Reapproved 2001), *Standard Test Method for In-plane Shear Response of Polymer Matrix Composite Materials by Tensile Test of a ±45° Laminate*, vol. 15.03, *Space Simulation; Aerospace and Aircraft; Composite Materials*. ASTM International, West Conshohocken, PA (2005).
52. D2344/D2344M-00^{e1}, 2005. *Standard Test Method for Short-Beam Strength of Polymer Matrix Composite Materials and their Laminates*, vol. 15.03, *Space Simulation; Aerospace and Aircraft; Composite Materials*. ASTM International, West Conshohocken, PA.
53. Whitney, J.M. 1985. Elasticity analysis of orthotropic beams under concentrated loads. *Composites Science and Technology*, 22, 167–184.
54. Whitney, J.M. 1989. Experimental characterization of delamination fracture, in Pagano, N.J. ed., *Interlaminar Response of Composite Materials, Composite Materials Series*, vol. 5, Pipes, R.B. (series ed.). Elsevier Science Publishers, Amsterdam, The Netherlands.
55. Whitney, J.M., Browning, C.E., and Hoogsteden, W. 1982. A double cantilever beam test for characterizing mode I delamination of composite materials. *Journal of Reinforced Plastics and Composites*, 1, 297–313.
56. D5528-01, 2005. *Standard Test Method for Mode I Interlaminar Fracture Toughness of Unidirectional Fiber-Reinforced Polymer Matrix Composites*, vol. 15.03, *Space Simulation; Aerospace and Aircraft; Composite Materials*. ASTM International, West Conshohocken, PA.
57. Russell, A.J. and Street, K.N. 1983. Moisture and temperature effects on the mixed mode delamination fracture of unidirectional graphite/epoxy, DREP Technical Memo 83–22, Defence Research Establishment Pacific, Victoria, B.C., Canada.
58. Russell, A.J. and Street, K.N. 1985. Moisture and temperature effects on the mixed mode delamination fracture of unidirectional graphite/epoxy, in Johnson, W.S. ed., *Delamination and Debonding of Materials*. ASTM STP 876, 349–370, American Society for Testing and Materials, Philadelphia, PA.
59. Carlsson L.A., Gillispie, J.W., Jr., and Pipes, R.B. 1986. On the analysis and design of the end notched flexure (ENF) specimen for mode II testing. *Journal of Composite Materials*, 20, 594–604.
60. D6671/D6671M-04^{e1}, *Standard Test Method for Mixed Mode I – Mode II Interlaminar Fracture Toughness of Unidirectional Fiber-Reinforced Polymer Matrix Composites*, volume 15.03, *Space Simulation; Aerospace and Aircraft; Composite*

61. Reeder, J.R. and Crews, J.H., Jr. 1990. Mixed mode bending method for delamination testing. *AIAA Journal*, 28(7), 1270–1276.
62. Reeder, J.R. and Crews, J.H., Jr. 1992. Redesign of the mixed mode bending delamination test to reduce nonlinear effects. *Journal of Composites Technology and Research*, 14(1), 12–19.
63. Liu, Z., Gibson, R.F., and Newaz, G.M. 2002. The use of a mixed mode bending test for characterization of mixed mode fracture behavior of adhesively bonded metal joints. *The Journal of Adhesion*, 78, 223–244.
64. Liu, Z., Gibson, R.F., and Newaz, G.M. 2002. Improved analytical models for mixed mode bending tests of adhesively bonded joints. *The Journal of Adhesion*, 78, 245–268.
65. Drzal, L.T., Rich, M.J., and Lloyd, P.F. 1982. Adhesion of graphite fibers to epoxy matrices: I. The role of fiber surface treatment. *Journal of Adhesion*, 16, 1–30.
66. Drzal, L.T., Rich, M.J., Koenig, M.F., and Lloyd, P.F. 1983. Adhesion of graphite fibers to epoxy matrices: II. The effect of fiber finish. *Journal of Adhesion*. 16, 133–152.
67. Drzal, L.T., Rich, M.J., and Subramoney, S. 1987. Fiber-matrix bonding and its effect on composite properties, in *Advanced Composites III — Expanding the Technology, Proceedings of the 3rd Annual Conference on Advanced Composites*, pp. 305–308. ASM International, Materials Park, OH.
68. McDonough, W.G., Herrera-Franco, P.J., Wu, W.L., Drzal, L.T., and Hunston, D.L. 1991. Fiber-matrix bond tests in composite materials, in *Advanced Materials/Affordable Processes, Proceedings of 23rd International SAMPE Technical Conference*, Kiamesha Lake, NY, pp. 247–258. Society for Advancement of Material and Process Engineering, Covina, CA.
69. Mandell, J.F., Grande, D.H., Tsiang, T.H., and McGarry, F.J. 1986. Modified microbonding test for direct in situ fiber/matrix bond strength determination in fiber composites, in Whitney J.M. ed., *Composite Materials: Testing and Design (Seventh Conference)*, ASTM STP 893, pp. 87–108. American Society for Testing and Materials, Philadelphia, PA.
70. Caldwell, D.L. 1987. Determination of the interfacial strength of composites, in *Advanced Composites III — Expanding the Technology, Proceedings of the 3rd Annual Conference on Advanced Composites*, pp. 299–303. ASM International, Materials Park, OH.
71. D2990-01, 2005. *Standard Test Methods for Tensile, Compressive, and Flexural Creep and Creep Rupture of Plastics*, vol. 08.01, *Plastics*, ASTM International, West Conshohocken, PA.
72. C 480-99 (Reapproved 2005). *Standard Test Method for Flexure Creep of Sandwich Constructions*, vol. 15.03, *Space Simulation; Aerospace and Aircraft; Composite Materials*. ASTM International, West Conshohocken, PA (2005).
73. Halpin, J.C. and Pagano, N.J. 1968. Observations on linear anisotropic viscoelasticity. *Journal of Composite Materials*, 2(1), 68–80.
74. Yeow, Y.T., Morris, D.H., and Brinson, H.F. 1979. Time-temperature behavior of a unidirectional graphite/epoxy composite, in Tsai S.W. ed., *Composite Materials: Testing and Design (Fifth Conference)*. ASTM STP 674, pp. 263–281. American Society for Testing and Materials, Philadelphia, PA.

76. Beckwith, S.W. 1980. Creep evaluation of a glass/epoxy composite. *SAMPE Quarterly*, 11(2), 8–15.
77. Irion, M.N. and Adams, D.F. 1981. Compression creep testing of unidirectional composite materials. *Composites*, 2(2), 117–123.
78. Lou, Y.C and Schapery, R.A. 1971. Viscoelastic characterization of a nonlinear fiber reinforced plastic. *Journal of Composite Materials*, 5, 208–234.
79. Gibson, R.F., Hwang, S.J., and Sheppard, C.H. 1990. Characterization of creep in polymer composites by the use of frequency-time transformations. *Journal of Composite Materials*, 24(4), 441–453.
80. Gibson, R.F., Hwang, S.J., Kathawate, G.R., and Sheppard, C.H. 1991. Measurement of compressive creep behavior of glass/pps composites using the frequency-time transformation method, in *Advanced Materials/Affordable Processes, Proceedings of 23rd International SAMPE Technical Conference*, pp. 208–218. Society for the Advancement of Material and Process Engineering, Covina, CA.
81. Gibson, R.F. and Kathawate, G.R. 1991. Rapid screening of creep susceptibility of structural polymer composites, in Stokes, V.J. ed., *Plastics and Plastic Composites: Material Properties, Part Performance and Process Simulation*, ASME MD vol. 29, pp. 161–171. American Society of Mechanical Engineers, New York.
82. D4065-01, 2005. *Standard Practice for Plastics: Dynamic Mechanical Properties: Determination and Report of Procedures, Volume 08.02 Plastics (II)*. ASTM International, West Conshohocken, PA.
83. E 756-05, 2005. Standard *Test Method for Measuring Vibration Damping Properties of Materials*, vol. 04.06, *Thermal Insulation; Environmental Acoustics*, ASTM International, West Conshohocken, PA.
84. Gibson, R.F. 1998. Vibration test methods for dynamic mechanical property characterization, in Jenkins, C.H. ed., *Manual on Experimental Methods for Mechanical Testing of Composites*, 2d ed., Chapter 14. Society for Experimental Mechanics, The Fairmont Press, Inc., Lilburn, GA.
85. Suarez, S.A. and Gibson, R.F. 1987. Improved impulse-frequency response techniques for measurement of dynamic mechanical properties of composite materials. *Journal of Testing and Evaluation*, 15(2), 114–121.
86. Dudek, T.J. 1970. Young's and shear moduli of unidirectional composites by a resonant beam method. *Journal of Composite Materials*, 4, 232–241.
87. Soovere, J. and Drake, M.L., 1985. *Aerospace Structures Technology Damping Design Guide: Volume I—Technology Review, AFWAL-TR-84-3089, vol. I.* Air Force Wright Aeronautical Labs, Wright-Patterson AFB, OH.
88. Suarez, S.A., Gibson, R.F., and Deobald, L.R., 1984. Random and impulse techniques for measurement of damping in composite materials. *Experimental Techniques*, M 8(10), 19–24.
89. Crane, R.M. and Gillispie, J.W., Jr. 1992. A robust testing method for determination of the damping loss factor of composites. *Journal of Composites Technology and Research*, 14(2), 70–79.
90. Deobald, L.R. and Gibson, R.F. 1988. Determination of Elastic Constants of orthotropic plates by a modal analysis/Rayleigh–Ritz technique. *Journal of Sound and Vibration*, 124(2), 269–284.

91. Ayorinde, E.O. and Gibson, R.F. 1993. Elastic constants of orthotropic composite materials using plate resonance frequencies, classical lamination theory and an optimized three mode Rayleigh formulation. *Composites Engineering*, 3(5), 395–407.
92. Gibson, R.F., Thirumalai, R., and Pant, R. 1991. Development of an apparatus to measure dynamic modulus and damping of reinforcing fibers at elevated temperature, *Proceedings 1991 Spring Conference on Experimental Mechanics*, pp. 860–869. Society for Experimental Mechanics, Bethel, CT.
93. Pant, R.H. and Gibson, R.F. 1996. Analysis and testing of dynamic micromechanical behavior of composite materials at elevated temperatures. *Journal of Engineering Materials and Technology*, 118, 554–560.
94. Mantena, R., Place, T.A., and Gibson, R.F. 1985. Characterization of matrix cracking in composite laminates by the use of damping capacity measurements. *Role of Interfaces on Material Damping*, pp. 79–93. ASM International, Materials Park, OH.
95. Mantena, R., Gibson, R.F., and Place, T.A. 1986. Damping capacity measurements of degradation in advanced materials. *SAMPE Quarterly*, 17(3), 20–31.
96. Gibson, R.F. 2000. Modal vibration response measurements for characterization of composite materials and structures. *Composites Science and Technology*, 60, 2769–2780.
97. Gibson, R.F., Srinivasan, N., Auner, G., Huang, C., Wang, Q., and Perooly, S. 2005. Vibration analysis of MEMS sensors for detection of ultrasound. *Proceedings of 2005 Society for Experimental Mechanics Conference*, Portland, Oregon, Paper # 279 on CD, Society for Experimental Mechanics, Bethel, CT.
98. Gibson, R.F., Ayorinde, E.O., and Wen, Y.-F. 2007. Vibrations of carbon nanotubes and their composites: a review. *Composites Science and Technology* 67(1), 1–28.

Appendix A

Stress Equilibrium Equations

For a body under static loading, the stresses at every point in the body must satisfy the static equilibrium conditions, $\Sigma\bar{F} = 0$ and $\Sigma\bar{M} = 0$, where $\bar{F}$ and $\bar{M}$ are the resultant external forces and moments, respectively, acting at the point. Consider the infinitesimal two-dimensional element of unit thickness shown in figure A1, where normal stresses are denoted by σ and shear stresses are denoted by τ.

The fact that the stresses in a body generally vary from point-to-point is accounted for by including differential changes in stresses from one face to another. For example, while the normal stress, σ_x, acts on the left face of the element, the variation of stresses from point-to-point is accounted for by assigning the normal stress, $\sigma_x + \frac{\partial \sigma_x}{\partial x} dx$, to the right face of the element (i.e., the stress, σ_x, changes at the rate $\frac{\partial \sigma_x}{\partial x}$ over the increment dx along the x direction). Similarly, the other stress components, σ_y, and τ_{xy}, must vary from the left face to the right face, and from the bottom face to the top face of the element. Now, the scalar component of the moment equilibrium condition, $\Sigma\bar{M}_O = 0$, at the center point O can be written as

$$\sum M_O = \tau_{xy} dy(1)\frac{dx}{2} + \left[\left(\tau_{xy} + \frac{\partial \tau_{xy}}{\partial x} dx\right) dy(1)\right]\frac{dx}{2} - \tau_{yx} dx(1)\frac{dy}{2}$$

$$-\left[\left(\tau_{yx} + \frac{\partial \tau_{yx}}{\partial y} dy\right) dx(1)\right]\frac{dy}{2} = 0$$

After dividing each term by $dxdy$, the remaining terms are

$$\tau_{xy} + \frac{\partial \tau_{xy}}{\partial x}\frac{dx}{2} - \tau_{yx} - \frac{\partial \tau_{yx}}{\partial y}\frac{dy}{2} = 0.$$

At a point in the body, where dx and dy both approach *zero*, the result is the proof of symmetry of the shear stresses

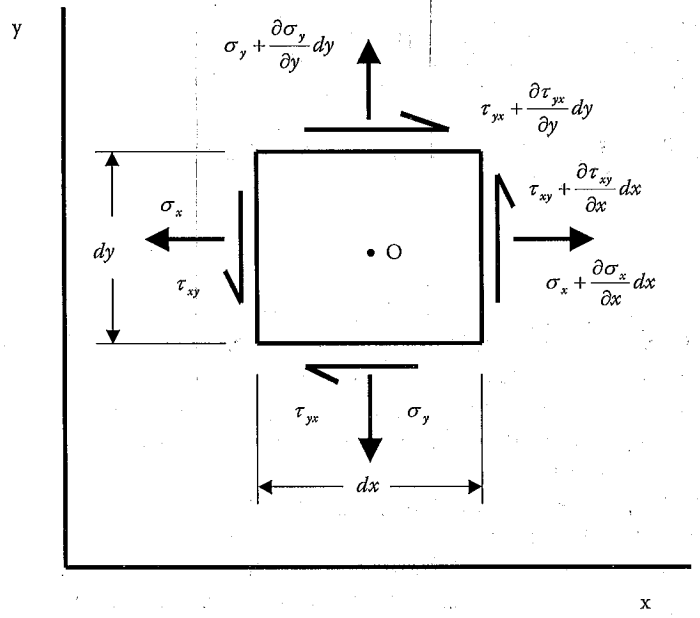

FIGURE A1
Infinitesimal element representing stresses at a point in a body.

and in the general 3D case,

$$\tau_{ij} = \tau_{ji}$$

where $i, j = 1, 2, 3$.

Thus, moment equilibrium requires that the shear stresses be symmetric. Recall that symmetry of the stresses was a key assumption leading to the development of the contracted notation in chapter 2.

Now with regard to the force equilibrium requirement, the scalar component of the force equilibrium condition $\Sigma \bar{F} = 0$ along the x direction is

$$\sum F_x = -\sigma_x dy(1) + \left(\sigma_x + \frac{\partial \sigma_x}{\partial x} dx\right) dy(1) - \tau_{yx} dx(1) + \left(\tau_{yx} + \frac{\partial \tau_{yx}}{\partial y} dy\right) dx(1) = 0$$

Simplifying the above equation, writing a similar equilibrium equation $\Sigma F_y = 0$, and making use of the symmetry condition $\tau_{xy} = \tau_{yx}$, we get the

2D stress equilibrium equations

$$\frac{\partial \sigma_x}{\partial x} + \frac{\partial \tau_{yx}}{\partial y} = 0$$

$$\frac{\partial \tau_{xy}}{\partial x} + \frac{\partial \sigma_y}{\partial y} = 0$$

A similar derivation for a 3D infinitesimal element including the force equilibrium requirement, $\Sigma F_z = 0$, leads to the full set of stress equilibrium equations

$$\frac{\partial \sigma_x}{\partial x} + \frac{\partial \tau_{yx}}{\partial y} + \frac{\partial \tau_{zx}}{\partial z} = 0$$

$$\frac{\partial \tau_{xy}}{\partial x} + \frac{\partial \sigma_y}{\partial y} + \frac{\partial \tau_{zy}}{\partial z} = 0$$

$$\frac{\partial \tau_{xz}}{\partial x} + \frac{\partial \tau_{yz}}{\partial y} + \frac{\partial \sigma_z}{\partial z} = 0$$

Appendix B

Strain-Displacement Equations

The relationships between strains and displacements at a point in a stressed body can be derived by considering the geometry of deformation of an infinitesimal element. Figure B1 shows the geometry of deformation for a 2D plane strain condition, where the original undeformed element is denoted by ABCD and the deformed element is denoted by A'B'C'D'.

So during deformation, point A deforms to point A', point B deforms to point B', and so forth. The displacement along the x direction is u, and the corresponding displacement along the y direction is v. Using the definition of normal strain (i.e., the change in length per unit length), for small deformations and strains, the normal strain along the x direction can be written as

$$\varepsilon_x = \frac{A'B' - AB}{AB} = \frac{\left[dx + \frac{\partial u}{\partial x}dx\right] - dx}{dx} = \frac{\partial u}{\partial x}$$

Similarly, the normal strain along the y direction is given by

$$\varepsilon_y = \frac{A'D' - AD}{AD} = \frac{\left[dy + \frac{\partial v}{\partial y}dy\right] - dy}{dy} = \frac{\partial v}{\partial y}$$

Referring to figure 2.2 and the definition of engineering shear strain, γ_{xy}, it is seen that γ_{xy} is equal to the difference between original right angle DAB in the undeformed element and the angle D'A'B' in the deformed element. If we assume small deformations and a correspondingly small angle between line A'B' and line AB, and define this small angle as θ, then we can write

$$\theta \cong \tan\theta = \frac{\partial v/\partial x}{dx}dx$$

Similarly, if we define the small angle between line A'D' and line AD as ϕ, we can write

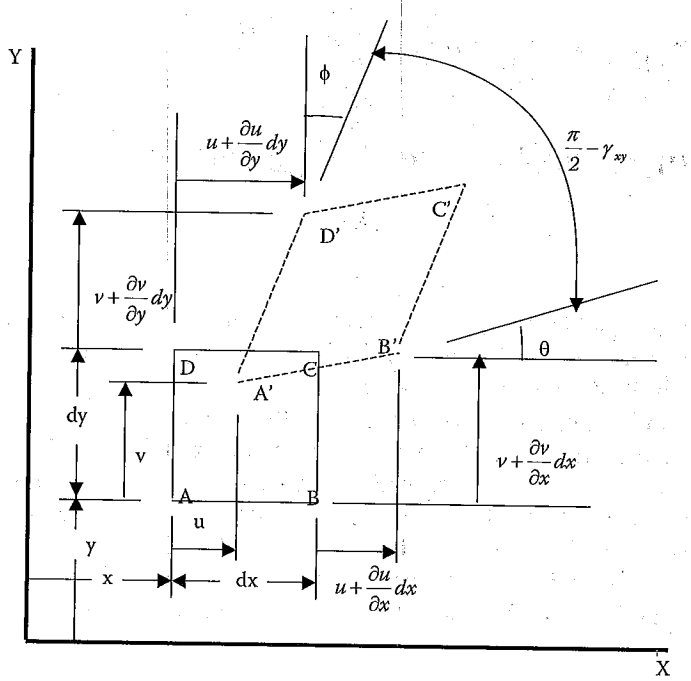

FIGURE B1
Geometry of deformation at a point in a stressed body. ABCD is undeformed element and A'B'C'D' is deformed element.

As a result, the shear strain is given by

$$\gamma_{xy}=\frac{\pi}{2}-\left[\frac{\pi}{2}-\theta-\phi\right]=\theta+\phi=\frac{\frac{\partial v}{\partial x}dx}{dx}+\frac{\frac{\partial u}{\partial y}dy}{dy}=\frac{\partial v}{\partial x}+\frac{\partial u}{\partial y}$$

In summary, the 2D strain-displacement equations are

$$\varepsilon_x=\frac{\partial u}{\partial x}$$

$$\varepsilon_y=\frac{\partial v}{\partial y}$$

$$\gamma_{xy}=\frac{\partial v}{\partial x}+\frac{\partial u}{\partial y}$$

Index

D

E

F

G

H

I

J

K

L

M

N

O

P

Q

R

S

T

U

V

W

Y

Z